FutureWater

teri THE ENERGY AND RESOURCES INSTITUTE

Utrecht University

UNIVERSITÉ DE GENÈVE

Developing a Glacio-Hydrological Model and IWRM Plan for a Selected Subbasin in the Central Himalayas, Uttarakhand, India

Present-day and future changes in the hydrology of the Bhagirathi Basin

REPORT

252

Present-day and future changes in the hydrology of the Bhagirathi Basin

Developing a Glacio-Hydrological Model and IWRM Plan for a Selected Subbasin in the Central Himalayas, Uttarakhand, India

Authors
Dr. Sonu Khanal (s.khanal@futurewater.nl)
Dr. Faezeh Nick (maghaminick@uu.nl)
Dr. Joel Fiddes (joel.fiddes@slf.ch)
Dr. Philip Kraaijenbrink (p.d.a.kraaijenbrink@uu.nl)
Prof. Dr. Walter Immerzeel (w.w.immerzeel@uu.nl)
Dr. Johannes Hunink (j.hunink@futurewater.nl)

Date
July 5 2022

Summary

In this report, we introduce the Spatial Processes in Hydrology (SPHY) model that we have used to assess upstream runoff composition in the Bhagirathi river basin. We use two model setups to evaluate the hydrological components of the whole Bhagirathi river basin (with the large scale model) as well as a more detailed analysis of a small catchment, the Din Gad catchment (the small scale model) in the Bhagirathi river basin. After calibrating and validating the model results for the baseline period (1991-2020), we assess the future hydrological changes of the selected basins. We selected a subset (4 GCM and two SSPs) of the full ensemble of climate change scenarios provided by General Circulation Models (GCMs) in the CMIP6 multi-model ensemble. The downscaled and bias-corrected GCM outputs are then used to force the SPHY model. This modeling study demonstrates how runoff composition and total runoff volume are expected to change by the end of the 21st century. Our results show that the total water availability for the whole Bhagirathi catchment will be relatively stable for ssp245 and slightly increases for ssp370 by the end of the century. However, there are considerable changes in the timing and magnitude of peak water availability and seasonality. This may impose a threat on the livelihood of the local communities if no adaptation measures are taken.

Content

Tables and Figures

1 Introduction

The Swiss Agency for Development and Cooperation's (SDCs) Global Programme Climate Change and Environment (GP CCE) India is supporting the operationalization of climate change adaptation actions in the mountain states of Uttarakhand, Sikkim and Himachal Pradesh through the phase two of the "Strengthening State Strategies for Climate Action" (3SCA) project that was launched in 2020. The second phase of 3SCA (2020-23), known as the Strengthening Climate Change Adaptation in the Himalayas (SCA-Himalayas), while building on the experience and achievements of Phase 1, aims to showcase mountain ecosystem appropriate scalable approaches for climate resilience in water and disaster risk management sectors; using these efforts to enhance the capacities of the institutions across the Indian Himalayan Region (IHR) to plan, implement and mainstream adaptation actions into their programmes and policy frameworks; and disseminating the experiences and lessons at the regional and global level. The project aims to develop and validate integrated approaches for climate resilient management of water resources and disaster risk (outcome 1), enhancing technical and institutional capacities to promote mainstreaming of climate resilient planning in water and disaster risk reduction (DRR) (outcome 2), and embedding integrated climate resilience approaches in water and DRR in the policy framework and to be replicated in other mountain regions (outcome 3).

This project presents a framework for Integrated Water Resources Management (IWRM) and Decision Support System (DSS) for the Himalayan subbasins consisting of three integrated platforms. (i) A modelling and decision support platform built around a multi-scale modelling framework for glacier-and snow-fed subbasins, based on state-of-the-art and "easy to use" modelling technology. (ii) A stakeholder engagement platform to consult key stakeholders, identify key IWRM issues and co-design a new IWRM plan for the Bhagirathi river basin. (iii) A capacity-building platform with on-site training and e-learning modules for the key project components: glacio-hydrological modelling, IWRM and DSS, to ensure the sustainability of the approach and pave the way for upscaling to other subbasins in the IHR.

To achieve the deliverables, the key tasks are structured in 4 work packages (Figure 1):

WP1: Glacio-hydrological modelling and climate change impact analysis for the Dokriani glacier catchment.
WP2: Integrated Water System Modelling platform and IWRM plan in the Bhagirathi river basin.
WP3: Guidelines for glacio-hydrological modelling, IWRM and DSS for IWRM in the Indian Himalayan Region context, and capacity building.
WP4: Project management and meetings.
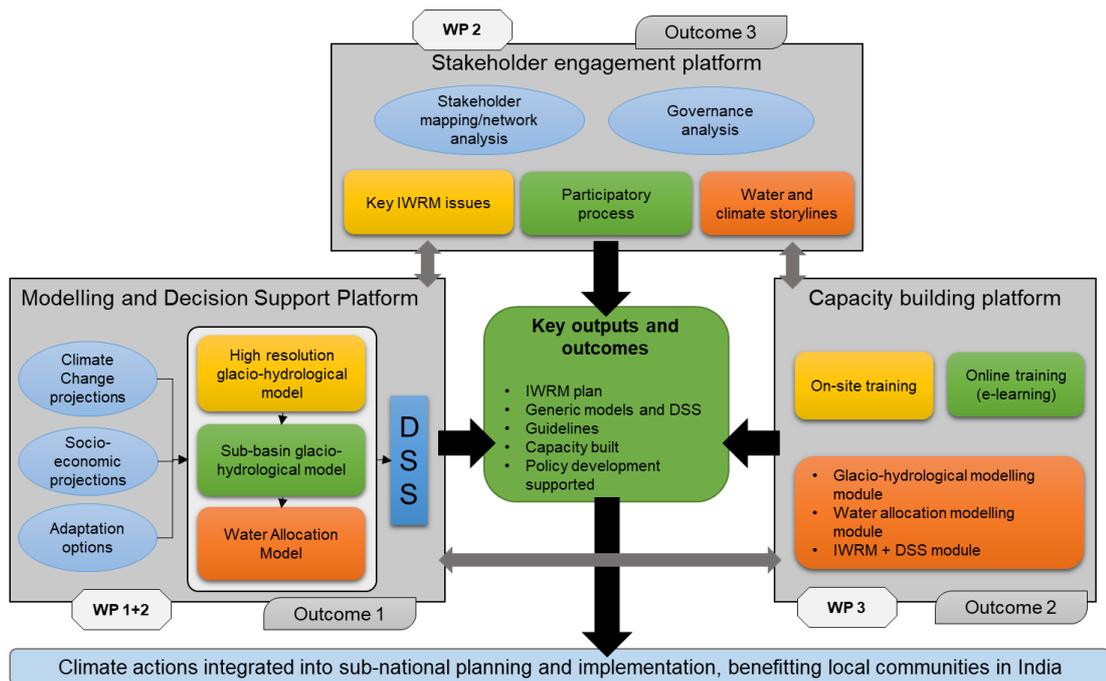
Figure 1. Project framework and subdivision of the key components.

To this end, this report presents the historical and future climate change impacts on the hydrological regime and water balance components of the water cycle in the Bhagirathi river basin and Din Gad catchment. The results of this report refer to the 'Outcome1' of the WP1 and WP2. Therefore, the objectives of this report are:

1. Understand the historical climate trends (precipitation and temperature), flow contributors and the key water balance components of the water cycle for the Bhagirathi river basin and Din Gad catchment.
2. Develop future climate change scenarios for the Bhagirathi river basin and Din Gad catchment.
3. Assess the future changes in water balance components at seasonal and decadal time scales in response to climate change for the Bhagirathi river basin and Din Gad catchment.

In this project, a large-scale Bhagirathi and a small-scale Din Gad glacio-hydrological models are set up to understand the impact of climate change on the water cycle at different temporal and spatial scales. The Bhagirathi model, which covers the entire upstream region just before its confluence with Alaknanda River at Devprayag, will focus on the changes in total water availability of the entire upstream region. Whereas the Din Gad model will focus on improving the understanding of the runoff contributors.

This report contributes to disentangling the aforementioned issues and helps to better understand the 21st-century climate change impacts on the water cycle of the region. The first chapter of this report describes the key component and the research objectives of the project. The second chapter describes the key features of two different study areas. The third chapter explains the model, data, and methodologies used for setting up the glacio-hydrological models. The fourth chapter presents the key results of this study. The fifth chapter discusses the limitations and key results of this study. Finally, the last chapter paves the way for upscaling the modelling approach used in this study to other subbasins in the IHR.

2 Study area

2.1 Bhagirathi river basin

The Bhagirathi[1] is a turbulent Himalayan river in the Indian state of Uttarakhand, and one of the two headstreams of the Ganges, the major river of Northern India and the holy river in Hinduism. The headwaters of the Bhagirathi are formed at Gaumukh (snout elevation 4000m), at the foot of the Gangotri and Khatling in the Garhwal Himalaya. The Bhagirathi and Alaknanda join at Devprayag in Garhwal and are thereafter known as the Ganges. The Bhagirathi basin, just before its confluence with Alaknanda at Devprayag, covers about an area of ~7642 Km^2.

The area has snow and glacier reserves that cover roughly 10% of its total area. A study by Raina et al. (2008) identified 238 glaciers of various shapes and sizes in the area. The distribution of these glaciers is uneven, with the highest number of glaciers located in the Bhagirathi river basin (78), followed by Jalandhar gad (64), Jahnvi/Jadh Ganga (60), Pilang (23), and Bhilangna (13). The Gangotri Glacier, which spans 144 square kilometers, is the largest glacier in the basin and the primary source of River Bhagirathi. The glacier alone contains an estimated 60% of the total ice volume of the glaciers in the valley (Raina et al., 2008). These glaciers are critical sources of freshwater and contribute significantly to the overall river runoff of Bhagirathi (Table A1). However, like other parts of the Himalayas, glaciers in the area are also retreating.

The Bhagirathi river basin is endowed with heterogeneous climatic conditions. The region, being situated centrally in the long sweep of the Himalayas, forms a transitional zone between the per-humid eastern and the dry to sub-humid western Himalayas. The northern part constitutes hilly topography, while the middle and southern parts are plain areas (Orr et al., 2019). The climate of the western Himalayas is influenced by two major climatic systems, the southwest Indian monsoon, and the northern hemispheric mid-latitude westerlies (Rai et al., 2014; Rehman et al., 2022). Most of the annual precipitation (1000-2500 mm per annum) in Garhwal occurs between July and September; during this time, the humid air masses of the Indian monsoon penetrate the high-altitude ranges of the Greater Himalayas. Rainfall magnitudes vary significantly both seasonally and across short distances (10^1 to 10^2 km) throughout the region, creating localized microclimates that are affected by the variability in terrain and geomorphic regime (Orr et al., 2019).

2.2 Din Gad catchment

The Din Gad valley is in the headwater region of the Bhagirathi rivre basin in the central Himalayas (Garhwal region, Uttarakhand, India). The catchment extends from 30° 48' to 32° 26 N and 76° 58 to 78° 51' E. It covers an area of 77.8 km2, extends from 2360 to 6632 m a.s.l. and about 9.6% of it is covered by glaciers (Thayyen and Gergan, 2010). Din Gad river emerges from Dokriani Glacier at an altitude of 3900 m a.s.l. and joins the Bhagirathi River near Bhukki village (
Figure **2**). The Dokriani Glacier is a valley glacier, 5 km long, ranging from 4050 (snout) to 6000 (Bergschrund) m a.s.l., with an area of 7.03 km2 (Figure A1).

The climate of the Din Gad catchment is humid-temperate in summer and humid cold in winter (Figure A2). The Din Gad catchment receives moisture from two sources: (i) by the Indian Summer Monsoon (ISM) that occurs during June–September and (ii) the western disturbances (WD) generally between December and March. Maximum solid precipitation (snow) also occurs from December to March due to WD (Thayyen et al., 2005; Yadav et al., 2018).

---

[1] Based on Wikipedia
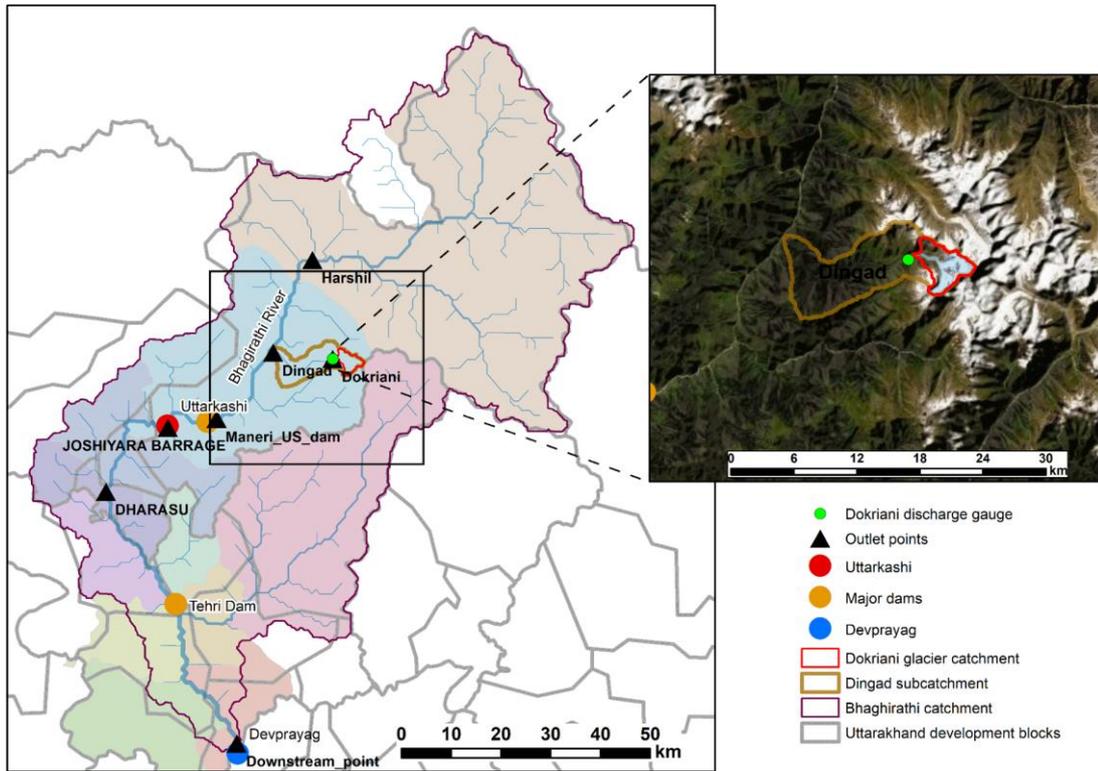
Figure 2. Bhagirathi river basin and the outlet points in the SPHY model. The observed discharge time series are available at Harshil, Maneri, Joshiyara and Dharasu. The inset shows Din Gad catchment and Dokriani Glacier.

3 Methodology

3.1 SPHY model

SPHY is a spatially distributed leaky bucket type of model and is applied on a cell-by-cell basis. The main terrestrial hydrological processes are described in a conceptual way so that changes in storages and fluxes can be assessed adequately over time and space. SPHY is written in the Python programming language using the PCRaster (Karssenberg et al., 2010) dynamic modeling framework.

SPHY is grid-based and cell values represent averages over a cell (Figure 3). For glaciers, sub-grid variability is considered: a cell can be glacier free, partially glacierized, or completely covered by glaciers. The cell fraction not covered by glaciers consists of either land covered with snow or land that is free of snow. Land that is free of snow can consist of vegetation, bare soil, or open water. The dynamic vegetation module accounts for a time-varying fractional vegetation coverage, which affects processes such as interception, effective precipitation, and potential evapotranspiration. Figure 4 provides a schematic overview of the SPHY modeling concepts.
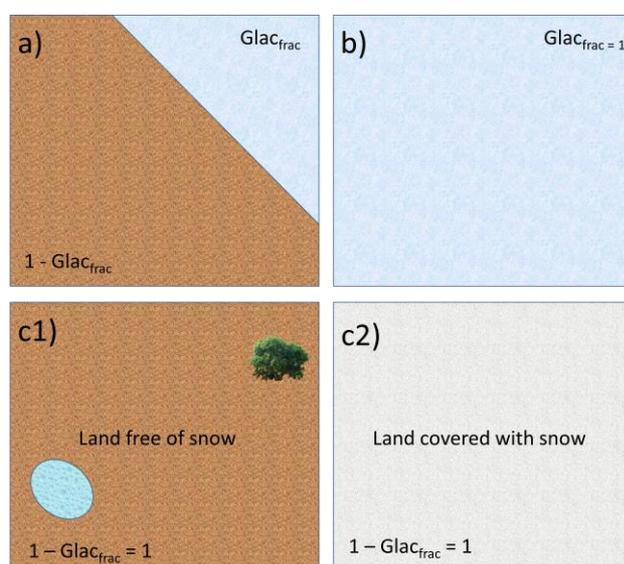
Figure 3. Illustration of SPHY sub-grid variability. A grid cell in SPHY can be (a) partially covered with glaciers, or (b) completely covered with glaciers, or (c1) free of snow, or (c2) completely covered with snow. In the case of (c1), the free land surface can consist of bare soil, vegetation, or open water.

The soil column structure is similar to VIC (Liang et al., 1994), with two upper soil storages and a third groundwater storage. Their corresponding drainage components are surface runoff, lateral flow and baseflow. SPHY simulates for each cell precipitation in the form of rain or snow, depending on the temperature. Precipitation that falls on land surfaces can be intercepted by vegetation and evaporated in part or whole. The snow storage is updated with snow accumulation and/or snowmelt. A part of the liquid precipitation is transformed in surface runoff, whereas the remainder infiltrates into the soil. The reference evapotranspiration is calculated using the Modified Hargreaves reference evapotranspiration method (Hargreaves and Samani, 1985). The resulting soil moisture is subject to evapotranspiration, depending on the soil properties and fractional vegetation cover, while the remainder contributes to river discharge by means of lateral flow from the first soil layer, and baseflow from the groundwater layer. The lateral flow, ground water storage, baseflow and their interaction are calculated as described in Terink et al., (2015).

Melting of glacier ice contributes to the river discharge by means of a slow and fast component, being (i) percolation to the groundwater layer that eventually becomes baseflow, and (ii) direct runoff. The cell-specific runoff, which becomes available for routing, is the sum of surface runoff, lateral flow, baseflow, snowmelt and glacier melt.

If no lakes are present, then the user can choose a simple flow accumulation routing scheme: for each cell, the accumulated amount of water that flows out of the cell into its neighboring downstream cell is calculated. This accumulated amount is the amount of water in the cell itself plus the amount of water in upstream neighboring cells of the cell and is calculated using the flow direction network. If lakes are present, then the fractional accumulation flux routing scheme is used; depending on the actual lake storage, a fraction of that storage becomes available for routing and is extracted from the lake, while the remaining part becomes the updated actual lake storage. The flux available for routing is routed in the same way as in the simple flow accumulation routing scheme.
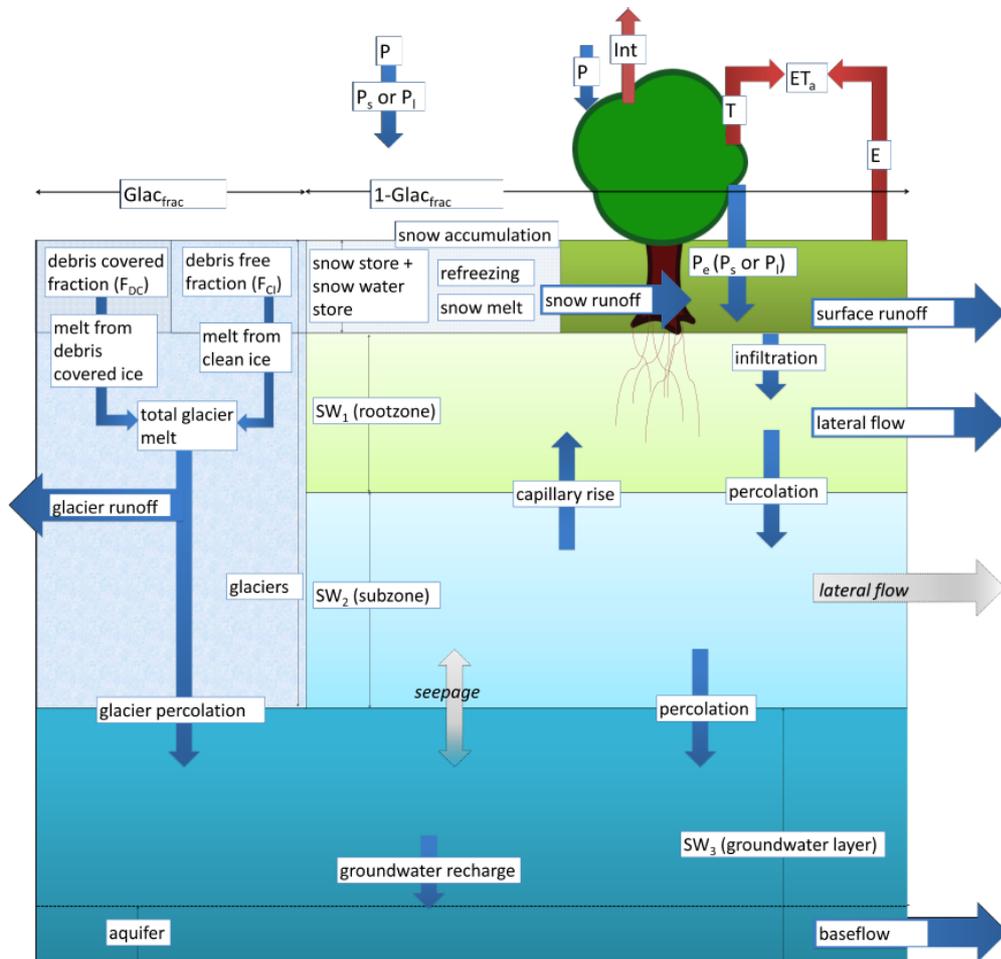
Figure 4. SPHY modeling concepts. The fluxes in grey are only incorporated when the groundwater module is not used.

The model source code is in the public domain (free access) and can be obtained from the SPHY model website free of charge (http://www.sphy-model.org). The two peer-reviewed open-access publications of the SPHY model can be found at https://doi.org/10.5194/gmd-8-2009-2015 (Terink et al., 2015) and https://doi.org/10.5194/esurf-6-687-2018 (Eekhout et al., 2018).

3.2 Dynamic Glacier Module

The model takes sub-grid variability into account to calculate the snow and glacier melt runoff from glaciers. By intersecting the glacier outlines, which each have a separate glacier ID, with the model grid the glaciers or parts thereof that lie within each model grid cell are identified (Kargel et al., 2014). Each (part of) glacier is assigned a unique ID. The glacier mass balance of each individual glacier, which can lie in multiple model grid cells is simulated to understand the future changes in glaciers. For each glacier, debris-covered and debris-free parts based is classified based on Kraaijenbrink et al., (2017). The initial ice thickness and volume for each glacier parts using data from Farinotti et al., (2019) are assigned in the next step. For each (part of) glacier the mean elevation from a 30x30 m digital elevation model is calculated (Farr et al., 2007). This is required to lapse daily air temperature from the model grid cell mean elevation to the glacier's mean elevation. Daily precipitation and temperature serve as input for the glacier module to calculate accumulation and melt. The module uses a degree-day approach to calculate the glacier ice melt with a degree-day approach (Hock, 2003). Different calibrated melt rates are applied to debris covered and debris free glaciers (Bolch et al., 2012; Gardelle et al., 2013; Scherler et al., 2011). Future changes in glacier fraction in response to the precipitation and temperature are considered by using a mass conserving ice distribution approach. The accumulated snow in the accumulation zone is transformed into ice and distributed downwards to the ablation area, at the end of each melting season (1st of October). The net imbalance (I), i.e., the difference in the volume of total snow accumulated (SnowS) and total volume of melt generated from the glaciers (GM), forms the basis of ice redistribution.

$$I_{n,j} = \mathrm{SnowS}_{n,j} - GM_{n,j} \qquad (1)$$

Where the subscript n is glacier id and j is a unique id. If the net imbalance is negative, then the volume of ice is redistributed ($Vred$) over the ablation zone.

$$Vred_{n,j} = \begin{cases} 0 & , \quad j\epsilon B_{n,j} \\ \sum_{j\epsilon B_{n,j}} I_{n,j} \times \dfrac{Vini_{n,j}}{\sum_{j\epsilon A_{n,j}} Vini_{n,j}}, & \quad j\epsilon A_{n,j} \end{cases} \qquad (2)$$

Where *Aj's are* the parts of the glacier with negative imbalance, *Bj's* are the parts of the glacier with a positive imbalance in any glacier id n. The redistribution is proportional to the initial total volume of ice ($Vini$). i.e., glacier parts with a larger initial ice volume will receive a large volume of accumulated ice from the accumulation zone to the ablation zone. The ice redistribution is done once a year (1st of October) at the end of the hydrological year (1st October to 30th September next year).

Similarly, a degree-day approach, with calibrated melt rates, is used to calculate the snow melt. Again, the precipitation and temperature drive the melting conditions. The model also allows refreezing of meltwater back into the snowpack. If the liquid snow exceeds the storage threshold, snow melt is generated.

3.3   Model Setup

We set up a detailed glacio-hydrological model for the Din Gad catchment that includes the Dokriani Glacier and a large catchment upstream of the Devprayag before its confluence with the Alaknanda River (Figure 2). A small-scale model (50 meters resolution) for the Din Gad catchment and a large-scale model (500 meters) for the Bhagirathi river basin are used in this project. We use the same climate data for both model setups. While the large-scale model is used to cover the whole area and study the fluxes at various locations, the small-scale model allows us to investigate different hydrological processes in detail and gain more insight into the role of different components in controlling the future streamflow in a warmer climate. Most importantly, we want to integrate the local scale information (for instance landuse characterstics, weather and climate, glacier mass balance, discharge data etc) with the small scale model to improve the understanding of the processes in the SPHY model.

3.4   Datasets

SPHY requires static data as well as dynamic data. For the static data, the most relevant are digital elevation model (DEM), land use type, glacier cover (including differentiation in debris-free and debris-covered ice surfaces), lakes/reservoirs and soil characteristics. The main dynamic data consist of climate data, such as precipitation, temperature, and reference evapotranspiration. Since SPHY is grid based, optimal use of remote sensing data and global data sources can be made. For example, the Normalized Difference Vegetation Index (NDVI) (Tucker 1979; Carlson and Ripley 1997; Myneni and Williams 1994) can be used to determine the leaf-area index (LAI) in order to estimate the growth stage of land cover.

3.4.1   Digital elevation model

The 1 arcsec (~30 m) Shuttle Radar Topography Mission (SRTM) digital elevation model (DEM) data are used (Farr et al., 2007). The DEM is resampled to 500m and 50m for the large-scale Bhagirathi and small scale Din Gad model.

3.4.2   Land use

Land use data used in the model are derived from the European Space Agency Climate Change Initiative (ESA CCI) data set (Kirches et al., 2014). The land use map is available for 300m resolution which is resampled to 500m for the Bhagirathi model. For the small-scale Din Gad model, a land use map is created using the Sentinel-2 image acquired on the 16th of October 2020 (Figure 5). The NDVI and NDSI are calculated from the image and then it is used to categorize land use classes. The final land use map has 7 classes as seen in Table 1. More than 50% of the Din Gad catchment is mainly covered by forest (mixed and dense combined). The glaciers (clean ice and debris) cover about 13% of the total catchment area.

Table 1. Landuse classes and its description for the Din Gad catchment

Class	Description	Area (Km^2)	Total Area (%)
1	Clean ice glacier	8.3	10.7
2	Debris covered glacier	2.1	2.7
3	Bare rock	1.7	2.1
4	Grass	10.6	13.6
5	Shrubs	14.6	18.8
6	Mixed forest	15.6	20.0
7	Dense forest	24.9	32.1
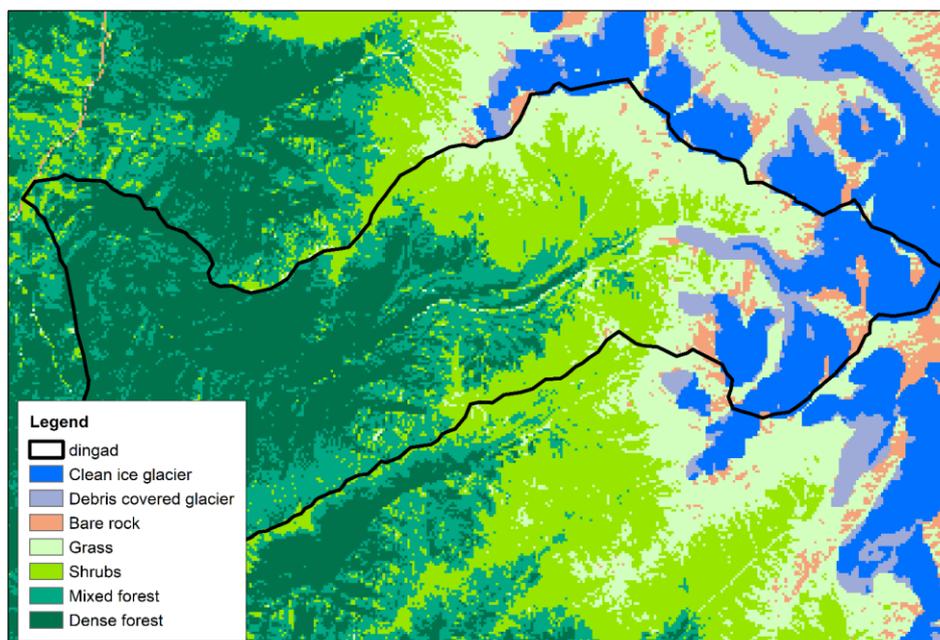
Figure 5. Landuse map generated for the Dingdad model.

3.4.3 Soil

Hydraulic soil properties used in this study were derived from HiHydroSoil (250m) and resampled to Bhagirathi and Din Gad model resolution (Simons et al., 2020).

3.4.4 Glacier mass balance

For the large-scale model, geodetic mass balance data from Shean et al., (2020) is used (Figure 6). This data base provides geodetic mass balance estimates for 99% of High Mountain Asia (HMA) glaciers between 2000 and 2018. For small scale Din Gad model, simulated data from Azam & Srivastava, (2020) and Dobhal et al., (2021) are used to calibrate the simulated glacier mass balance on Dokriani Glacier.
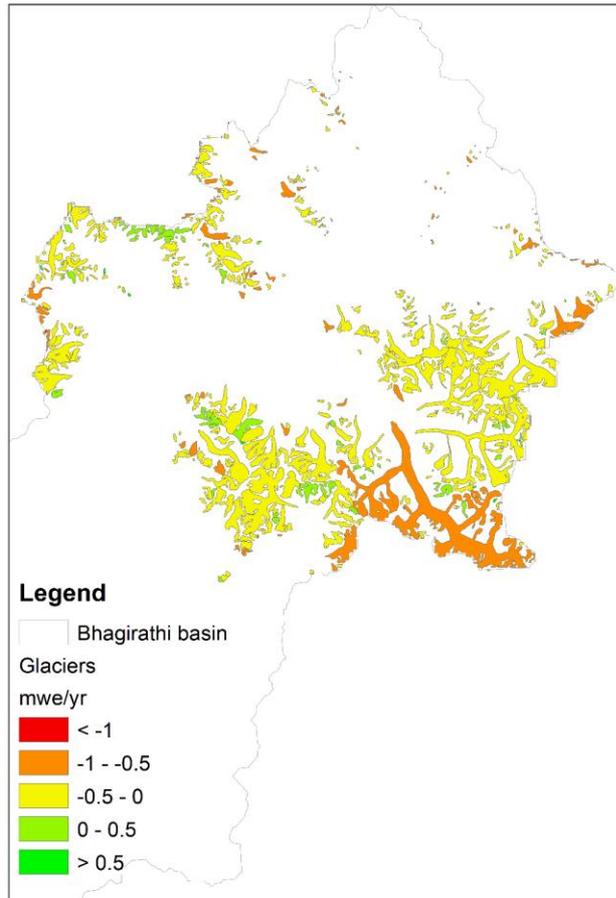
Figure 6. Geodetic glacier mass balance data from Shean et al (2020).

3.4.5 Snow cover

The MODIS MOD10CM006 (500m) snow cover data (2001–2017) is used to calculate the monthly snow persistence (Hall and Riggs, 2015) for the large-scale Bhagirathi model.
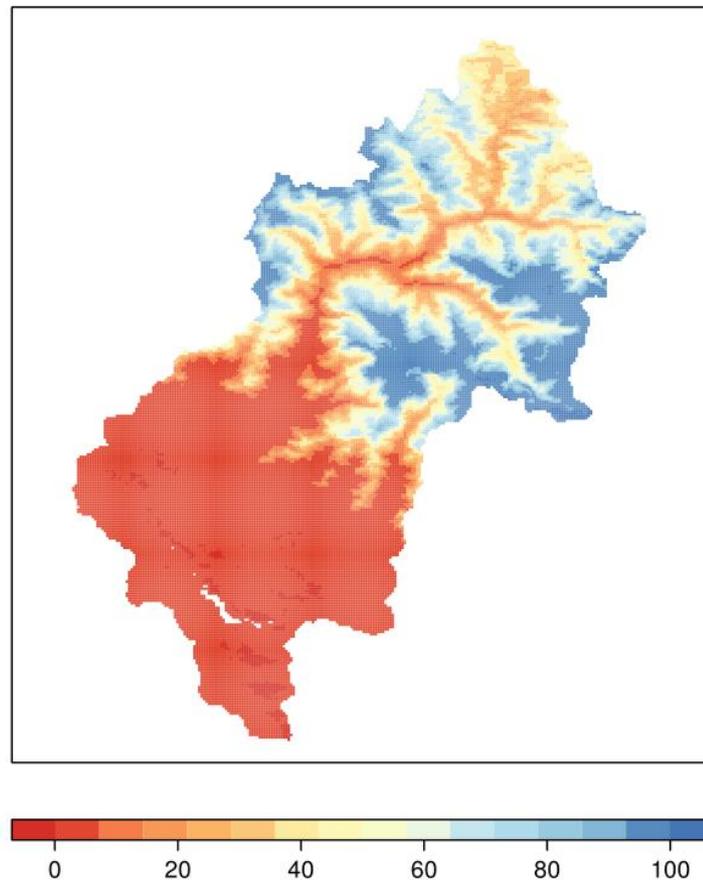
Figure 7. MODIS snow persistence map for the Bhagirathi river basin for the period 2001–2017.

3.4.6 Meteorological data

The meteorological forcing for SPHY has been provided by the topography-based downscaling scheme TopoSCALE (Fiddes and Gruber, 2014). TopoSCALE downscales atmospheric fields available on pressure levels to a high-resolution digital elevation model. In this case, the atmospheric model data is provided by the latest generation of ECMWFs reanalysis product, ERA5 (Hersbach et al., 2020).

TopoSCALE performs a 3D interpolation of atmospheric fields available on pressure levels, to account for time-varying lapse rates, and a topographic correction of radiative fluxes. The latter includes a cosine correction of incident direct shortwave radiation on a slope, adjustment of diffuse shortwave and longwave radiation by the sky view factor, and elevation correction of both longwave and direct shortwave. It has been extensively tested in various geographical regions and applications, e.g., permafrost in the European Alps (Fiddes et al., 2015), permafrost in the North Atlantic region (Westermann et al., 2015), Northern hemisphere permafrost (Obu et al., 2019), Antarctic permafrost (Obu et al., 2020), Arctic snow cover (Aalstad et al., 2018), Arctic climate change (Vikhamar Schuler and Østby, 2020) and Alpine snow cover (Fiddes et al., 2019). TopoSCALE can therefore provide hillslope scale model forcings without any requirement for ground data by accounting for the main topographic effects on atmospheric forcing. In this project, we developed a plugin for the SPHY model which produces gridded forcing fields, accounts for projection differences between the target grid and native ERA5 (WGS84) and produces forcing files in SPHY required format. We generated SPHY forcings for the period 1991-2020 and these data have been further used as a baseline dataset with which to downscale CMIP6 climate data.

3.4.7 Streamflow

Table 2. Observed discharge stations in the study area

Station	Resolution	Start	End	Years	Missing data (%)
Harshil	Hourly	2017	2020	4	32
Maneri	daily	2016	2021	6	0
Joshiyara	daily	2008	2019	12	0
Dharasu	daily	2016	2021	6	31[1]

There are 4 discharge stations in the Bhagirathi river basin as shown in Figure 2. Since the discharge stations at Harshil and Dharasu have more than 30% missing data, we use the station data at Maneri and Joshiyara to calibrate the Bhagirathi model. The other two stations, i.e., Harshil and Dharasu, will be used for the independent validation. Moreover, there are some abstractions from the main Bhagirathi rivers as the discharge measured at Dharasu is less compared to that measured in Joshiyara Barrage. We do not include this water abstraction in the SPHY model and will be explicitly modeled in the Water Evaluation and Planning (WEAP) model. Since there are no observed stations available in the upstream part of the Bhagirathi river basin, the Din Gad model is calibrated based on the modeled outputs from Azam and Srivastava, (2020). The modeled output from Azam and Srivastava, (2020) (here after 'observed' only for the Din Gad model) is available for the period 2000–2020.

3.5 Model calibration and validation

Glacio-hydrological model calibration can suffer from equifinality (Azam et al., 2021). Equifinality is the phenomenon that different parameter combinations can lead to the same simulated discharge pattern. For example, a shortage in snow melt can be compensated by excess glacier melt. To avoid the pitfalls of model equifinality, we use a three-step modeling strategy to calibrate the snow, glaciers, and rainfall-runoff processes in the model (Khanal et al., 2021; Pellicciotti et al., 2012). First, parameters related to glacier processes are calibrated to observed glacier mass balance data. Second, parameters related to snow are calibrated to MODIS snow persistence. Finally, rainfall-runoff and routing parameters are calibrated to observed streamflow. Reliable calibration to multiple observed variables ensures that the processes are accurately represented in the model and helps to build confidence and trust with the end-users that the tools are robust in the Indian Himalayan context.

3.6 Future climate change scenarios

Future climate forcings for this study are based on new Coupled Model Intercomparison Projects phase 6 (CMIP6) ensembles. CMIP6 consists of the "runs" from around 100 distinct climate models being produced across 49 different modeling groups. The number of climate models is large and computational and human resources are limited; therefore, it is necessary to compromise the number of climate models that can be included in our future climate study.

3.6.1 Model selection

The selection of climate models is not straightforward and can be done by following different methods. Here we use an approach explained by Lutz et al., (2016) to select climate models combining the envelope approach and the past-performance approach. The goal is to select an ensemble consisting of a manageable number of climate model runs, which still represents all potential future scenarios in terms of future mean air temperature and annual precipitation sums, and only includes models with acceptable performance in simulating the historical climate.

We have used two scenarios, (SSP2-RCP4.5) and a more extreme one (SSP3-RCP7.0). For each, we select 4 GCMs representing 4 corners of the envelope (cold, wet / cold, dry / warm, wet / warm, dry). EC-Earth3 and EC-Earth-CC are included. Other EC-Earth variants are excluded. We have selected only GCM runs that have daily mean air temperature, daily maximum air temperature, daily minimum air temperature, and daily precipitation. Only models that have data available at a daily time step are selected because this is a requirement for an empirical – statistical downscaling method to be applied to the GCM runs at a later stage.

Changes in climatic means of the initial selection is based on the range of projections of changes in mean air temperature (ΔT) and annual precipitation sum (ΔP) between 1985 – 2014 and 2071 – 2100, averaged over the GCM grid cells covering the basin, in native spatial resolution of each GCM. For the model runs included in RCP4.5 and RCP7.0 separately, the 10th and 90th percentile values for ΔT and ΔP are determined after resampling all GCM data to the same grid. These values represent the four corners (wet/warm, dry/warm, wet/cold, dry/cold) of the spectrum of projections for temperature and precipitation change. The 10th and 90th percentiles are chosen rather than the minimum and maximum projections to avoid selecting outliers, cf. other studies (e.g., Immerzeel et al., 2013; Sorg et al., 2014). The proximity of the model runs to the 10th and 90th percentiles are derived from the model runs' percentile rank scores corresponding to their projections for ΔT and ΔP with respect to the entire range of projections in the entire ensemble:

$$D_{P_i^T, P_i^P} = \sqrt{((|P_i^T - P_j^T|)^2 + (|P_i^P - P_j^P|)^2)}$$

where $D_{P_i^T, P_i^P}$ is the distance of a model (j)'s ΔT and ΔP (P_j^T, P_j^P, respectively) to the corner (i)'s 10th and/or 90th percentile score of ΔT and ΔP for the entire ensemble (P_j^T, P_j^P, respectively).

3.6.2 Downscaling

To bias correct the future CMIP6 GCM temperature and precipitation forcing and downscale it to the model domain grid, we applied a monthly delta change approach. Climatological monthly mean differences (i.e., deltas) over 1991–2020 between the baseline data and each GCM were applied to the entire daily future GCM series (2021–2100) by, for each individual day, using the delta corresponding to the same month of the year.

4 Results

4.1 Present-day climatology

4.1.1 Bhagirathi domain

The climate of the Bhagirathi is influenced by two major climatic systems, the southwest Indian monsoon, and the northern hemispheric mid-latitude westerlies. Precipitation amounts vary significantly along the North-South transect in the Bhagirathi Basin (Figure 8a). The northern and northeastern regions are drier compared to the wetter southern part. The differences in precipitation patterns are attributed to the steep topography of the region. The latitudinal stretch of the Himalayas obstructs the orographic influence of precipitation in the south and southeastern part thus making the northern and northeastern regions drier. As a result, the precipitation within the Bhagirathi Basin shows a high annual variability of the precipitation ranging from 1900 mm yr^{-1} in the southern and western parts to 500 mm yr^{-1} in the northern parts (Figure 8a; 8c). The years 2010 and 2009 received the maximum and minimum annual precipitation of about 1780 mm and 1070 mm, respectively. There are no visible significant trends for the basin aggregated annual precipitation in the Bhagirathi Basin (shown by the red dashed line). The basin also shows high monthly variability of the precipitation (Figure 8e). The months of July and November receive the maximum and minimum precipitation of about 320 mm and 22 mm, respectively. The monsoon period (June through September) dominates the seasonal precipitation distribution and comprises 64% of the annual precipitation.

The northern region is colder compared to the southern parts (Figure 8b). The basin shows a high annual variability of the annual average temperature ranging from -15.7 to 20.6 °C (Figure 8d). 2016 and 1997 are the hot (6.1 °C) and the cold (3.7 °C) years, respectively. In contrast to precipitation, the annual average temperature shows a visible significant increasing trend of 0.017 °C yr^{-1}. This cumulates to a 0.52 °C temperature rise in the basin over the past 30 years. The monthly temperature shows a distinct seasonal cycle where the temperature is higher for the monsoon months compared to the winter months (Figure 8f). The average temperature is highest for July (11.3 °C) and lowest for January (-2.6 °C). The largest variability in the basin aggregated monthly average temperature is found in the winter months (December, January, and February).
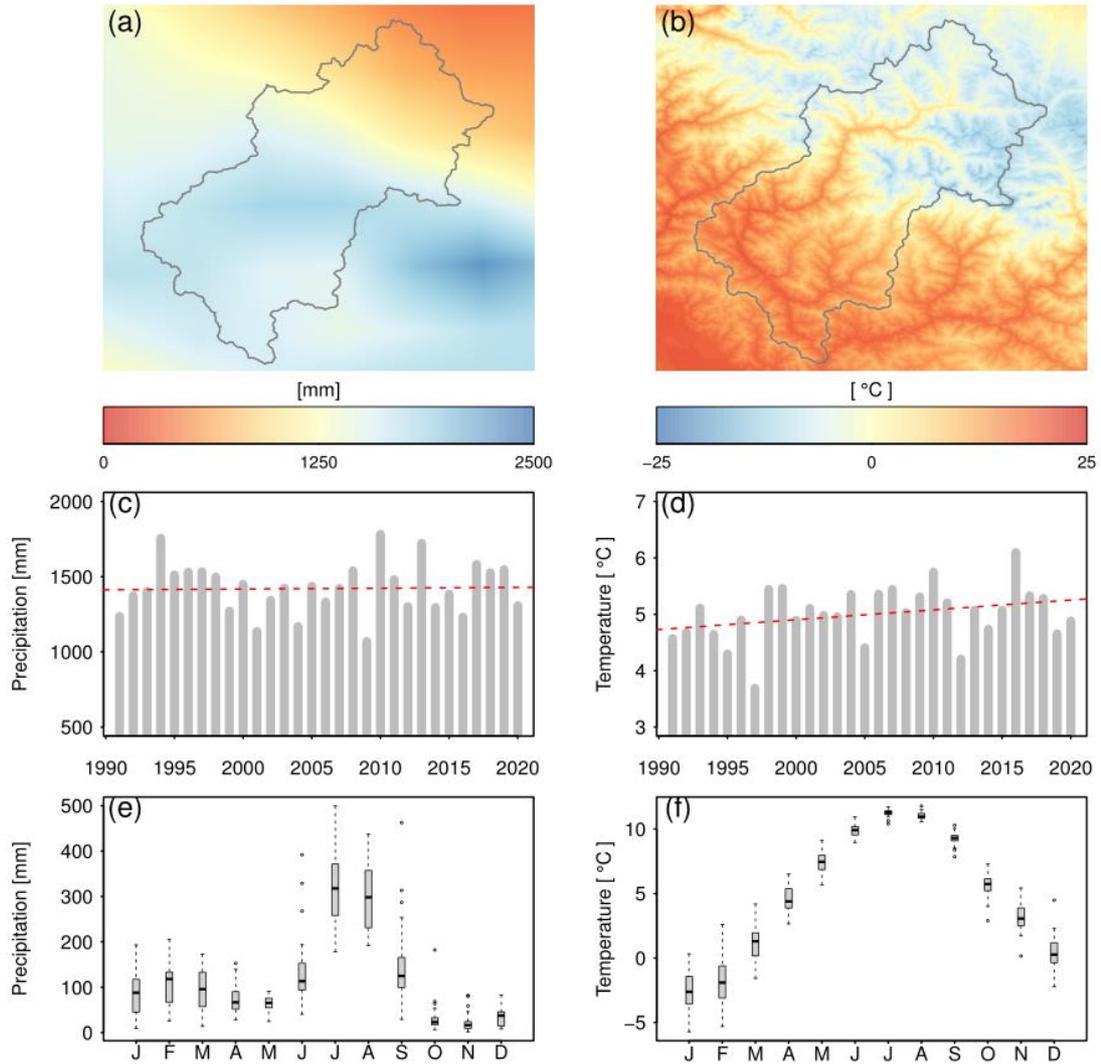
Figure 8. The historical downscaled climate (ERA5 with TopoSCALE) of the Bhagirathi model domain for the baseline period (1991–2020). (a) mean annual precipitation, (b) average temperature, (c) mean annual average precipitation aggregated over the domain, (d) mean annual average temperature aggregated over the domain, (e) climatology of the precipitation, and (f) climatology of the average temperature.

4.1.2   Din Gad domain

Similar to the Bhagirathi domain the precipitation over the northern part is less compared to the precipitation in the southern part of the Din Gad domain (Figure 9a). The precipitation within the Din Gad catchment ranges from 1667 mm yr^{-1} in the northern parts to 1808 mm yr^{-1} in the southern and western parts (Figure 9a). The basin shows a higher annual variability of the precipitation compared to the Bahagirathi basin (Figure 9c). The years 2013 and 2009 received the maximum and minimum annual precipitation of about 2300 mm and 1328 mm respectively. In contrast to the Bhagirathi domain, the precipitation shows an increasing trend of 6.8 mm yr^{-1}. The seasonal patterns of precipitation are similar to the Bhagirathi domain and monsoon comprises 60% of the annual precipitation (Figure 9e).

The average annual temperature within the basin ranges from -12.5 to 13.6 °C (Figure 9b). 2016 and 1997 are the hot (2.54 °C) and the cold (-0.13 °C) years respectively (Figure 9d). The annual average temperature for the Din Gad domain shows a higher warming trend of 0.024 °C yr^{-1} compared to the

Bhagirathi domain. This cumulates to a 0.73 °C temperature rise in the basin over the past 30 years. The largest variability in the monthly average temperature is found in the winter months (Figure 9f). The basin average temperature is highest for July (8.3 °C) and lowest for January (-6.5 °C).
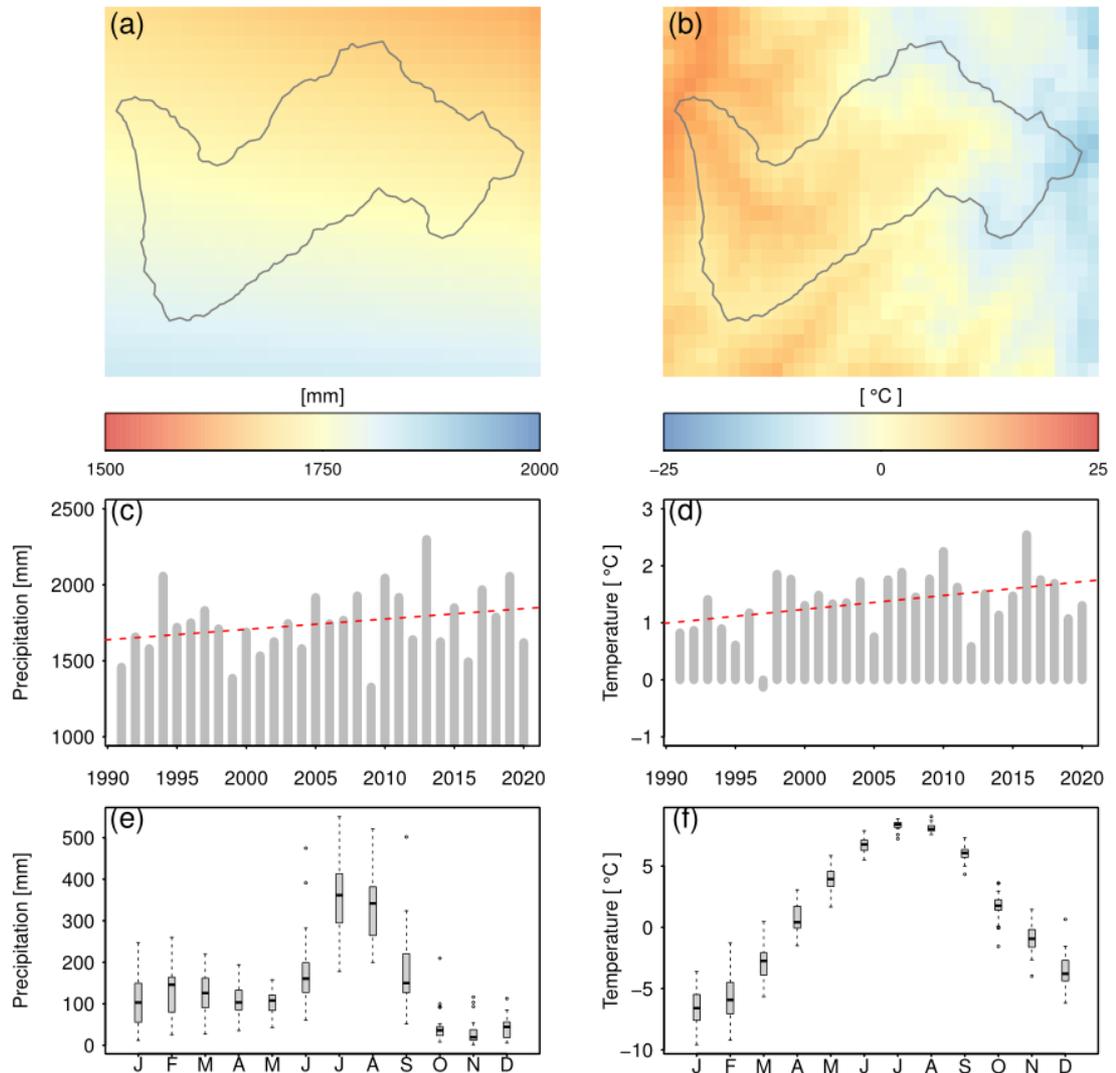
Figure 9. The historical climate (ERA5 with TopoSCALE) of the Din Gad model domain for the baseline period (1991–2020). (a) mean annual precipitation, (b) average temperature, (c) mean annual average precipitation aggregated over the domain, (d) mean annual average temperature aggregated over the domain, (e) climatology of the precipitation, and (f) climatology of the average temperature.

4.2   Model calibration

4.2.1   Glacier mass balance

To calibrate the SPHY model for the Bhagirathi river basin, the geodetic mass balance data from Shean et al (2020) is used (referred to as geodetic mass balance data through out the study). This dataset provides consistent geodetic mass balance estimates for 99% of HMA glaciers between 2000 and 2018. Since, there were no spatially consistent observed large scale glacier mass balance database available for the entire Bhagirathi river basin, we chose to use geodetic mass balance data to ensure spatial consistency in the model. The Bhagirathi SPHY model is simulated for the same period (2000–2018) to calculate the glacier mass balance. The parameters related to glacier mass balance, i.e., DDFS (degree day factor for snow), DDFG (degree day factor for clean glaciers), DDFDG (degree day factor for debris

covered glaciers), SnowSC (water that can be stored in the snow pack), and temperature and precipitation are fine-tuned. Some parameters, for instance DDFG and Trcit (critical temperature for the melt), are adapted from Azam and Srivastava, (2020). A spatial precipitation correction factor, based on model simulation, is also calibrated for all the galciers over the region. A precipiation correction alone was not sufficient to calibrate the glacier module in the model. Moreover, several studies have found a cold bias in ERA5 temperature in mid-latitudes and on the Tibetan Plateau (Cao et al., 2020; Ji and Yuan, 2020; Orsolini et al., 2019; Yan et al., 2019). Therefore, we adjusted the temperature based on the simulated glacier mass balance from SPHY and geodetic mass balance data from Shean et al (2020). A temperature correction of +1°C (for entire Bhagirathi river basin), based on model simulations, is found for the large-scale Bhagirathi domain. Figure 10 shows the glacier mass balance of all the glaciers within the Bhagirathi river basin compared to the geodetic mass balance. The parameters used in the glacier module of the Bhagirathi SPHY model are calibrated for all the individual glaciers in the region. It is ensured that the mass balance of Dokriani, Gangotri, and any glacier larger than 2 km^2 is in line with the available geodetic dataset (Shean et al., 2020). The final simulated glacier mass balance for 2000–2018 for Dorkrani glacier (computed from the Bhagirathi SPHY model) is -0.009 m.w.e yr^{-1} which is in good agreement with -0.049 m.w.e yr^{-1} as found in the geodetic mass balance data. However some studies suggested a larger mass loss of -0.27 m w.e. yr^{-1} over 2000–2018 (based on model simulations) (Azam and Srivastava, 2020), -0.23 ± 0.1 m w.e. yr^{-1} for 1999–2014 (based on geodetic mass balance calculated from Cartosat-1) (Garg et al., 2022) and -0.34 ± 0.2 m w.e. yr^{-1} (based on glaciological measurement) (Garg et al., 2022) for Dokriani glacier. However, such simulated, geodetic and observed mass balance datasets are not available consistently for the whole Bhagirathi river basin domain. Considering the lack of consistent data availability on the Bhagirathi river basin scale and the uncertainty associated with the mass balance, it is concluded that the glacier mass balance calibration of the Bhagirathi SPHY model is realistic and satisfactory for use in further analysis.
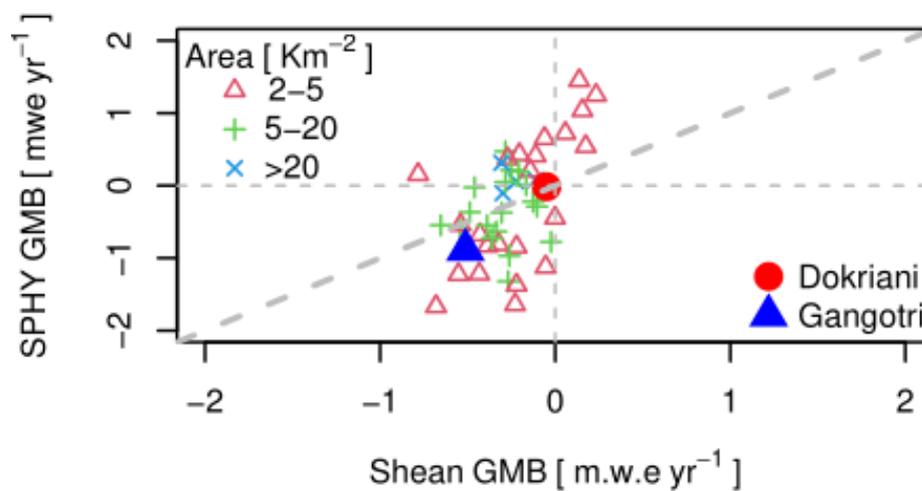
Figure 10. Average annual glacier mass balance in m.w.e yr-1 for all the glaciers within the Bhagirathi river basin. The grey inclined dashed line shows the 1:1 line.
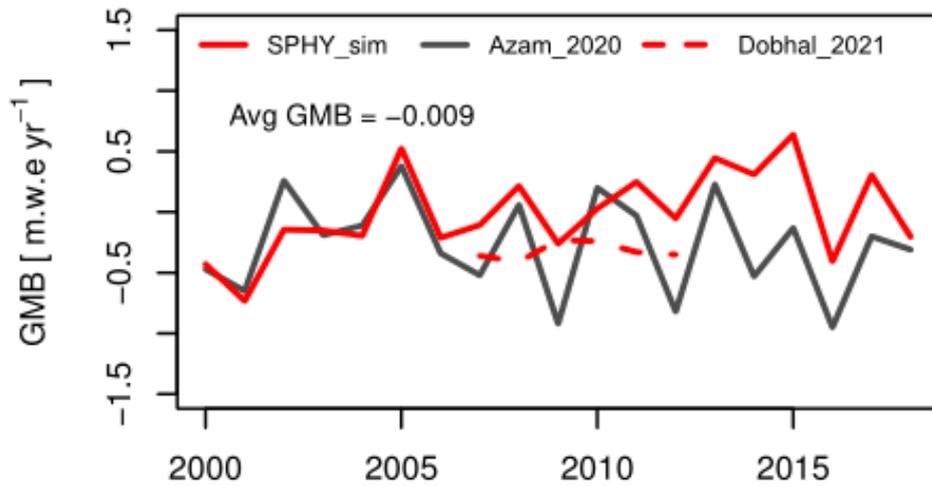
Figure 11. Annual glacier mass balance time series of the Dokriani glacier (from Bhagirathi SPHY model). The red line is simulated glacier mass balance from SPHY, the black line is simulated data from Azam & Srivastava, (2020) and the red dashed line from Dobhal et. al, 2021.

To further calibrate the model for the Din Gad domain, the annual glacier mass balance time series of the Dokriani Glacier from the small-scale SPHY model is compared with the simulated mass balance data from Azam and Srivastava, (2020), Srivastava et al., (2021) and measured mass balance data from Dobhal et al., (2021). By fine-tuning the ERA5 temperature data, increase of 2.5° C based on model simulation, the model can simulate the annual mass balance in a comparable range with the mass balance data from the previous studies (Figure 12).
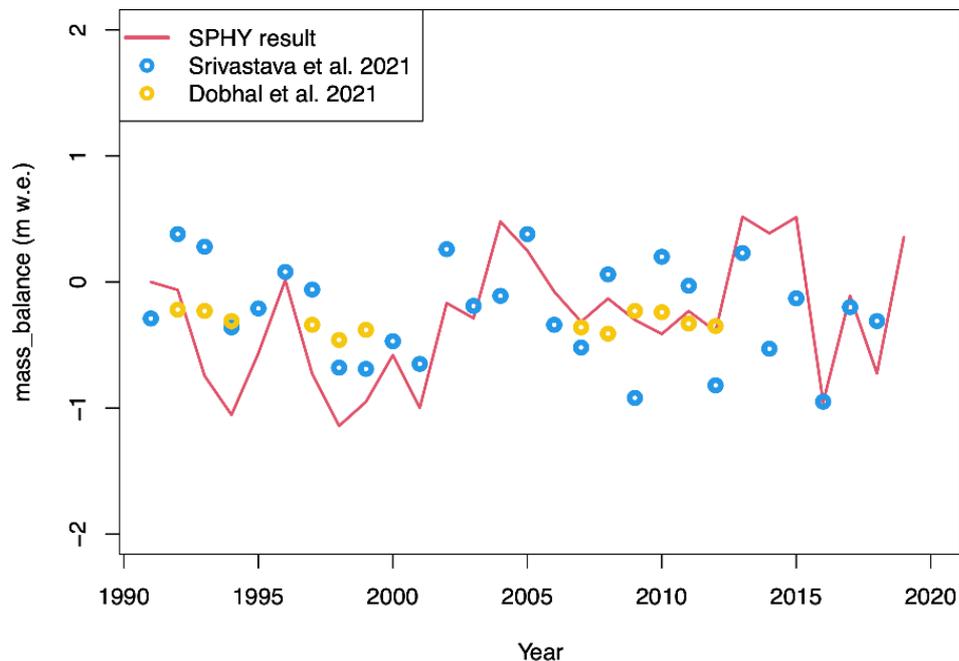
Figure 12. Annual glacier mass balance time series of the Dokriani glacier. The red line is a simulated glacier mass balance from SPHY (the small scale model). Blue and yellow circles are simulated data from Srivastava et al. 2021 and measured data from Dobhal et al. 2021, respectively.

4.2.2   Snow validation

The snow in the Bhagirathi SPHY model is validated with MODIS snow data (Hall et al., 2002). The snow persistence, i.e., % of the time a pixel is covered with snow, is calculated for the SPHY and MODIS for

2001–2017. The difference in snow persistence between SPHY and MODIS reveals that the snow is slightly overestimated at the higher altitudes in the modelled Bhagirathi river basin (Figure 13a). The Bhagirathi SPHY model snow persistence matches well below 4000m elevation (Figure 13b). The overestimation in the snow persistence from the Bhagirathi SPHY model comes from the winter and post-monsoon (October and November) months (Figure 13c). This overestimation in snow persistence can be attributed to the cold bias (maximum of +5 °C over the TP region) in the ERA5 data which has been reported in the past studies (Khanal et al., 2021; Yan et al., 2019). Overestimation of snow cover extent could potentially lead to an overestimation of snow runoff calculation. Given the scarcity of the snow-related data in the region (such as, snow redistribution and avalanching), a realistic modeling of sublimation is not possible. Moreover, the actual snowmelt calculation depends on the snow water equivalent (SWE), which depends on snowfall. Though, there are spatial differences between observed and modeled snow cover, at the basin scale this effect will be less pronounced. On the Bhagirathi river basin scale, the average aggregated annual changes in snow persistence from the Bhagirathi SPHY model and MODIS are well below 10% threshold (Figure 13d).
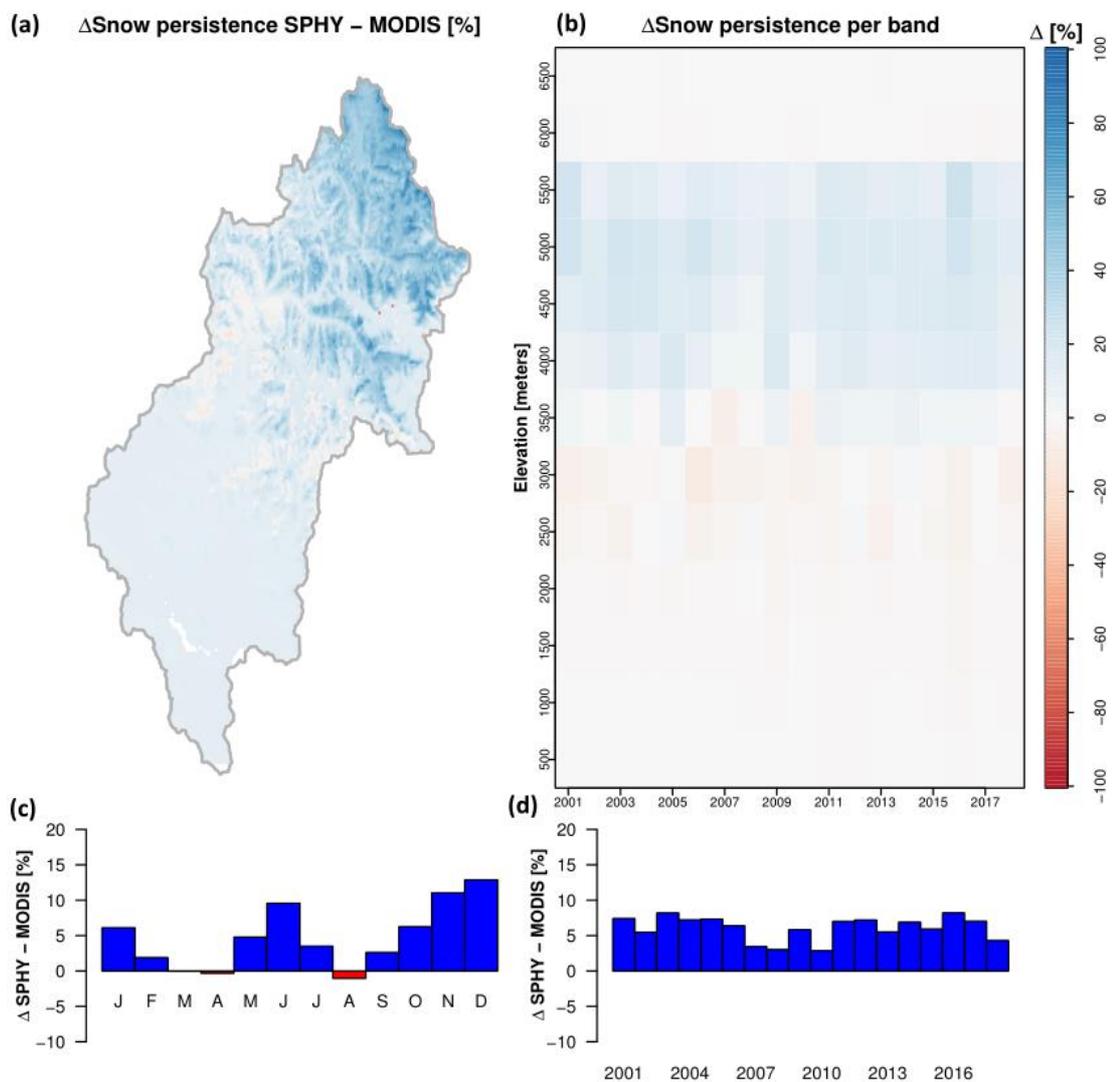
Figure 13. Snow persistence validation for the Bhagirathi SPHY model. (a) changes in snow persistence in SPHY and MODIS data, (b) snow persistence changes per elevation band in the basin, (c) basin aggregated monthly snow persistence and (d) annual time series of changes in snow persistence.

4.2.3   Stream flow calibration

To calibrate the rainfall-runoff parameter, the observed daily stream flow datasets are used. The parameters such as soil depth (root depth and sub-depth), groundwater (alphaGW and deltaGW), and routing (Kx) are fine-tuned to match simulated runoff with observed streamflow data (Table 3). Since the observed daily discharge time-series data were not sufficiently long enough (2016–2020 for the Maneri and 2016–2019 for Joshiyara station) for the split-sample test, the Maneri station is chosen for the calibration and Joshiyara as the independent validation station. To estimate the efficiency of the calibration to stream flow, the Nash-Sutcliffe efficiency criterion (NSE), percent bias (PBIAS), and coefficient of determination (R^2) are used as performance indicators (Nash & Scliffe, 1970).

At the daily scale in Maneri, the PBIAS, NSE, and R^2 are found to be 15.3, 0.77, and 0.82 (Figure 14). The discharge calibration at the daily scale in the Bhagirathi river basin is found to be "Very good" (Moriasi et al., 2007). There is a slight overestimation of the flow at Maneri (15.3%) for the calibration period and even higher at the validation station Joshiyara (17.7%) (Figure 15). The overestimation in discharge can most likely be attributed to the overestimation in precipitation amounts in ERA5 in the HMA region (Khanal et al, 2021). Further, extremely large rainfall totals, to some extent, can be attributed to "rain bombs" in the numerical weather prediction model (NWP) used in ERA5 (Harrigan, 2020). The discharge calibration shows the hydrological regime at Maneri and Joshiyara is melt-dominated as 60.6% of the total runoff is contributed by snow and glaciers. The snow runoff is the dominant source of runoff at Maneri (50%) and Joshiyara (44%). Considering the close agreement of runoff totals, contributions compared to past studies, uncertainties in the ERA5 input data, and the large spatial model domain, it is concluded that the model performance is satisfactory for further analysis.
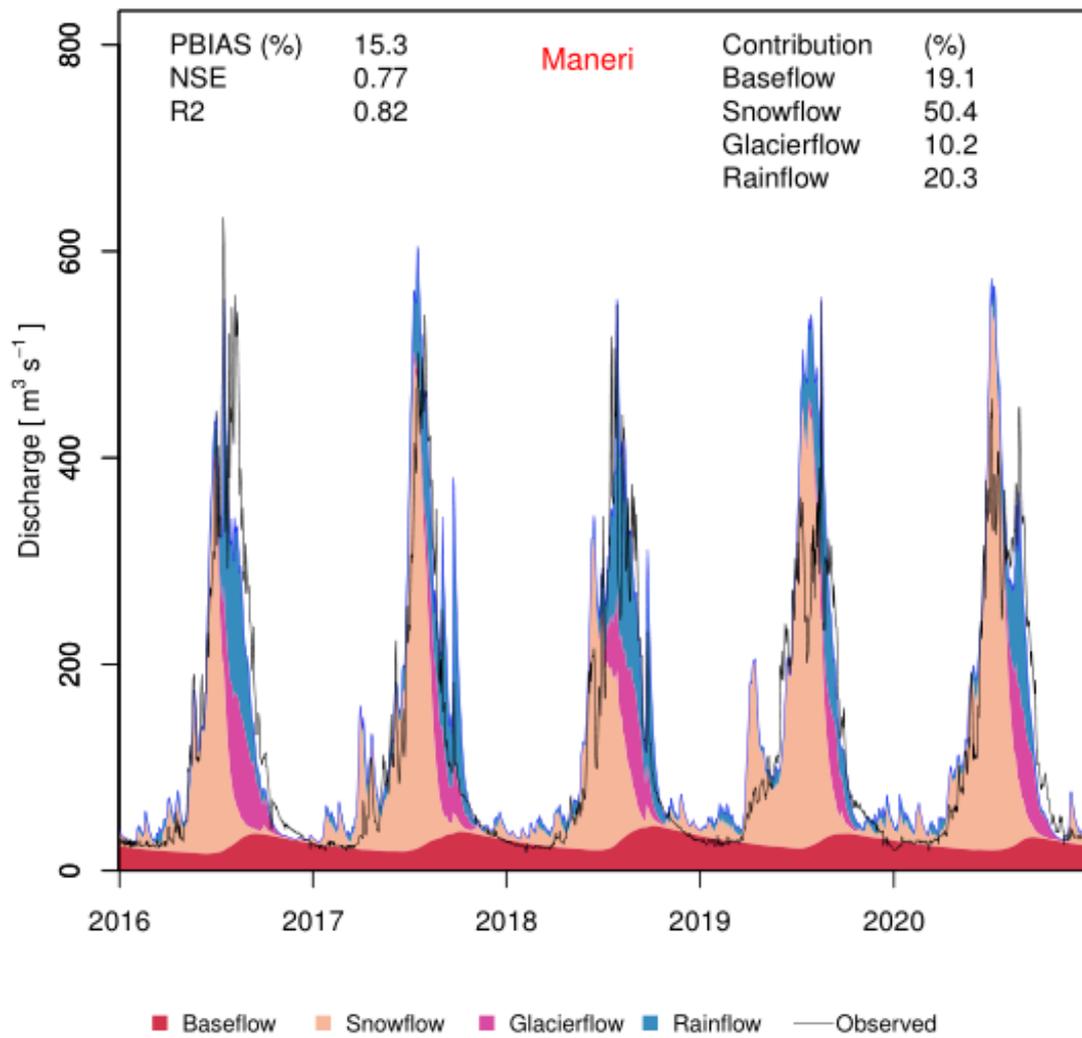
Figure 14. Observed and simulated discharge with the distinction of flow components (base, snow, glacier and rain-runoff flow at calibration location, Maneri, shown in Figure 2 for 2016–2020. Top left part of the figure shows values for model performance indicators; percent bias (PBIAS), Nash-Sutcliffe efficiency criterion (NSE) and coefficient of determination (R^2) at the top left corner. The top right part of the figure shows the contribution of stream flow contributors to the total flow (expressed in %).
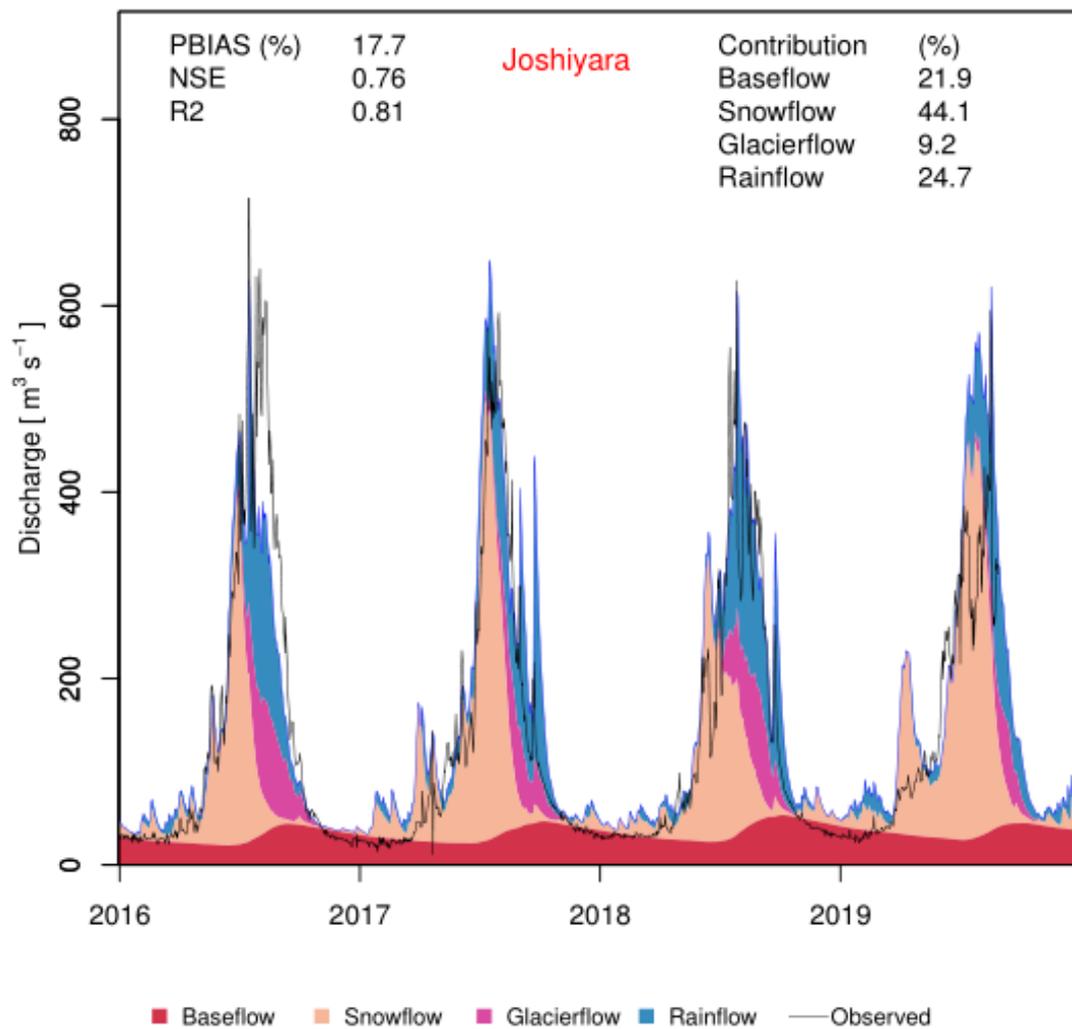
Figure 15. Observed and simulated discharge with the distinction of flow components (base, snow, glacier and rain-runoff flow at validation location, Joshiyara, shown in Figure 2 for 2016–2020. The top left part of the figure shows values for model performance indicators; percent bias (PBIAS), Nash-Sutcliffe efficiency criterion (NSE) and coefficient of determination (R^2) at the top left corner. The top right part of the figure shows the contribution of stream flow contributors to the total flow (expressed in %).

Table 3. Final calibrated SPHY model parameters

Parameters	Description	Units	Value
DDFS	Degree day factor for Snow	mm °C^{-1} day^{-1}	6.1
DDFDG	Degree day factor for debris cover glacier	mm °C^{-1} day^{-1}	4.8
DDFG	Degree day factor for Snow for glacier	mm °C^{-1} day^{-1}	7.7
Tcrit	Critical temperature	°C^{-1}	0.7
SnowSC	Water storage capacity of snow pack	-	0.5
Kx	Routing recession coefficient	-	0.9
RootDepthFlat	Thickness of root zone	mm	300
SubDepthFlat	Thickness of subsoil	mm	150
alphaGw	Baseflow recession coefficient	-	0.5
YieldGw	Specific aquifer yield	-	0.05

We further validated the results from the small-scale model, comparing our results with available simulated and measured data from the Dokriani catchment. Even though the outlet from this catchment

has been studied since 1992, continuous records are not available since the measurements have been affected by frequent floods in the valley. We have gathered measured data for summer months from previous studies by Thayyen et al., (2005) and Kumar et al., (2014), and further we compared our results with the simulated results from Azam and Srivastava, (2020). There is an underestimation in discharge of about 16,7% compared to the simulated results from Azam and Srivastava, (2020). This underestimation can most likely be attributed to the underestimation in precipitation amounts in ERA5 in high altitude in the HMA region. Note that our results here are compared to the modelled results from Azam and Srivastava (2020), which were tuned to reach the amount of flux from the limited observed data. Such an approach has been used in other studies (Khanal et al., 2021; Lutz et al., 2014; Wijngaard et al., 2017). Figure 16 shows that for the Dokriani catchment, glacier runoff contributes to 21% of the total flux. While snow and rain runoff contribute to about 68%, which agrees with the previous studies (Azam and Srivastava, 2020; Thayyen et al., 2007).
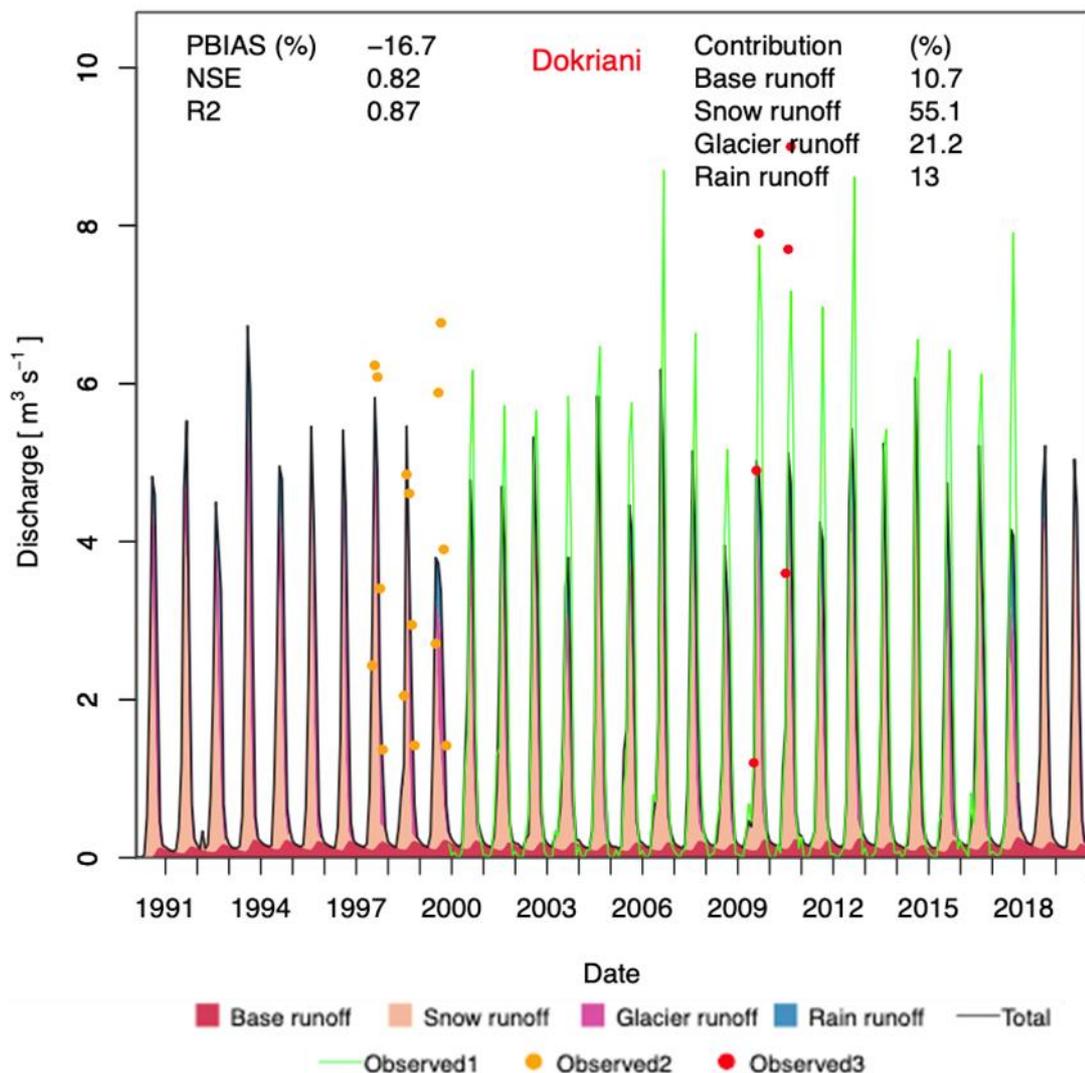
Figure 16. Observed and simulated discharge for Dokriani catchment. Modelled data are shown with the distinction of flow components (base, snow, glacier and rain runoff). Observed 1,2 and three are simulated data from Azam and Srivastava 2020, observed data from Thayyen et al 2004 and Kumar et al 2014, respectively. The values for model performance indicators; percent bias (PBIAS), Nash-Sutcliffe efficiency criterion (NSE) and coefficient of determination (R2) at the top left corner is calculated using observed1. The top right part of the figure shows the contribution of stream flow contributors to the total flow (expressed in %).

4.3 Present-day hydrology

The parameters from fine-tuned Bhagirathi SPHY model are used to understand the changes in baseline hydrological fluxes between 1991–2020 period. At the outlet of the Bhagirathi River, just before the Alaknanda River, the rainfall-runoff is the dominant contributor to the the total runoff (Figure 17). Rainfall-runoff contributes all-round the year and provides about 33.8% of water (the total flow) to the river system. The rainfall-runoff contribution starts to increase rapidly from June and peaks in the month of August, similar to the monsoon landfall timing in the region as discussed in the section 4.1.1. The contribution of rainfall ceases rapidly after the monsoon. The second-largest contributor is snow runoff and contributes about 31.3% of the total runoff. Although the snow contributes all-round the year, most of the snow melt starts from March/April and snow runoff peaks in July when most of the precipitation falls as snow over the high elevation of the Bhagirathi river basin. The snow contribution again ceases in the winter season when the temperature is low and solid form of precipitation is stored as snow over the higher elevation. The glacier contributes to about 5.7% to total runoff. The glacier melts when the temperature is above zero on the glacier surface. The glacier melt starts in May and peaks in August. Even though the annual contribution of glacier is smallest at the outlet its monthly contribution reaches 14.6% in September when there is less water in the river system. The baseflow drains water to the river channel all-round the year but its contribution increases in the dry and cold season (September, October, November, December, January, February) and overall contributes to about 29.2% to the total flow.

Figure 17. Baseline averaged monthly runoff with the distinction of flow components (base, snow, glacier, and rain-runoff flow at the outlet of the Bhagirathi river basin (just before the confluence of the Alaknanda River) for 1991–2020. The top right part of the figure shows the contribution of stream flow contributors to the total flow (expressed in %).

The baseline hydrological fluxes for the Dokriani catchment are shown in Figure 18. Snow and glacier runoff are the main contributors to the total flux of Dokriani catchment since it is located at higher elevation and is more glacier and snow fed. Glacier runoff contributes to about 20% of the total flux. The main contributor is the snow runoff which contributes about 55% of the total flux. Snow runoff starts from March/April, and it peaks in the beginning of July. The snow runoff reduces in September and October as the temperatures get negative in higher elevations and snow melt does not occur. The third contributor is rain runoff, contributing to 13% of the total flux. Rain runoff starts to increase in June and peaks in August.
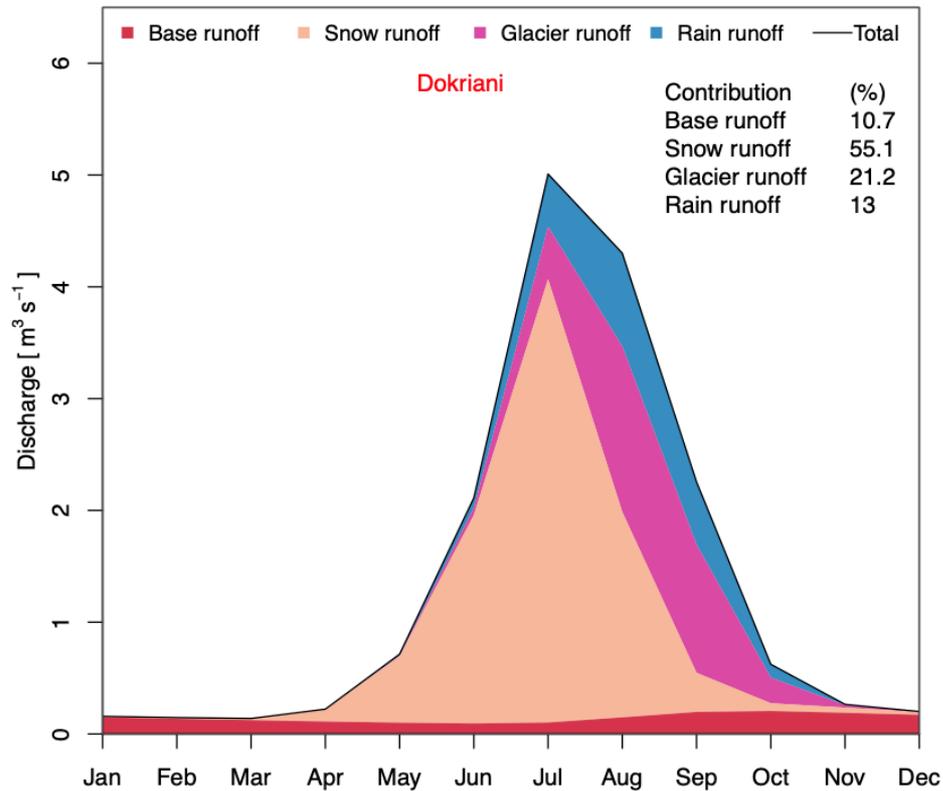
Figure 18. Baseline averaged monthly runoff with the distinction of flow components (base, snow, glacier, and rain-runoff) at the Dokriani outlet for 1991–2020. The top right part of the figure shows the contribution of stream flow contributors to the total flow (expressed in %).

The spatial runoff patterns reveal that the snow and glacier melt runoff contribution is high for the upstream river reaches of the basin (Figure 19). The glacier melt contribution is > 80% for the river reach originating from the Gangotri Glacier. Whereas the snow melt contribution is larger for the river reaches above Harshil and the Jadh Ganga. The Din Gad catchment is mainly dominated by the snowmelt runoff and rainfall-runoff components. Again, the upstream river reaches of the Bhilangana River, the other major tributary of the Bhagirathi River, are dominated by snow and glacier melt. For the lower part of the basin, the flow is dominated by the rainfall-runoff and the baseflow components.
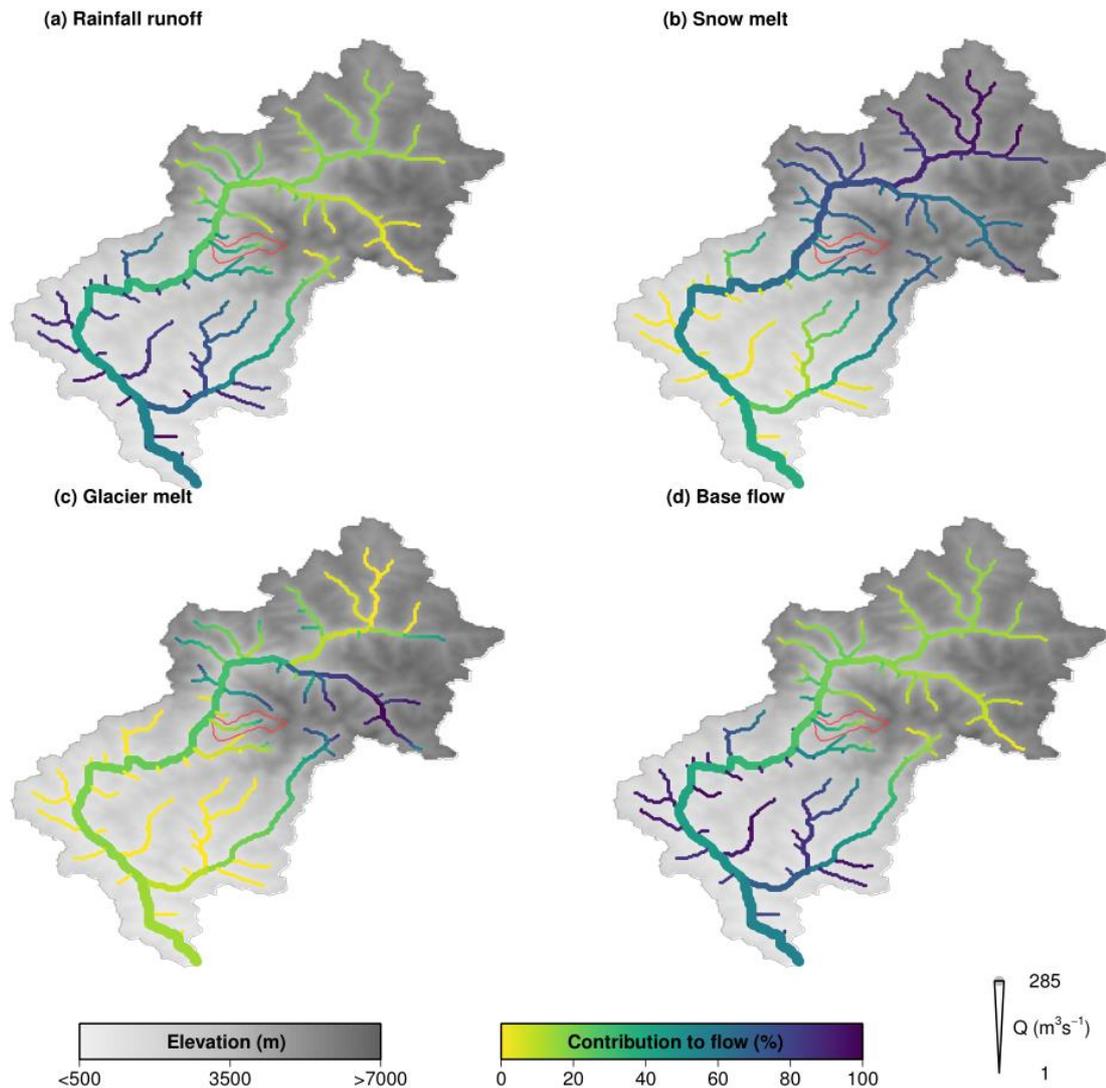
Figure 19. Spatial patterns of the flow components (base, snow, glacier, and rain-runoff) at the outlet of the Bhagirathi river basin (just before the confluence of the Alaknanda river) for 1991–2020. The grey and red boundary represent the Bhagirathi river basin and Din Gad catchment.

There is large annual variability in the flow hydrograph patterns for the Bhagirathi river basin (Figure 20). The variability is associated with the physiographic and climatic characteristics, such as variability in precipitation, temperature, changes in glacier ice reserves over the seasons and years. The maximum peak total flow in the baseline period is found to be 2163 cumecs in June 2013. The modelled peak discharge timing aligns with reported flooding in the Uttarakhand state. This is one of the worst natural disasters when widespread heavy rains resulted in floods across the Uttarakhand state, claiming thousands of lives and damage worth billions of rupees. This flash flood event was triggered by very heavy rainfall and cloudburst in the Uttarakhand region (Houze et al., 2017; Kumar, 2013).
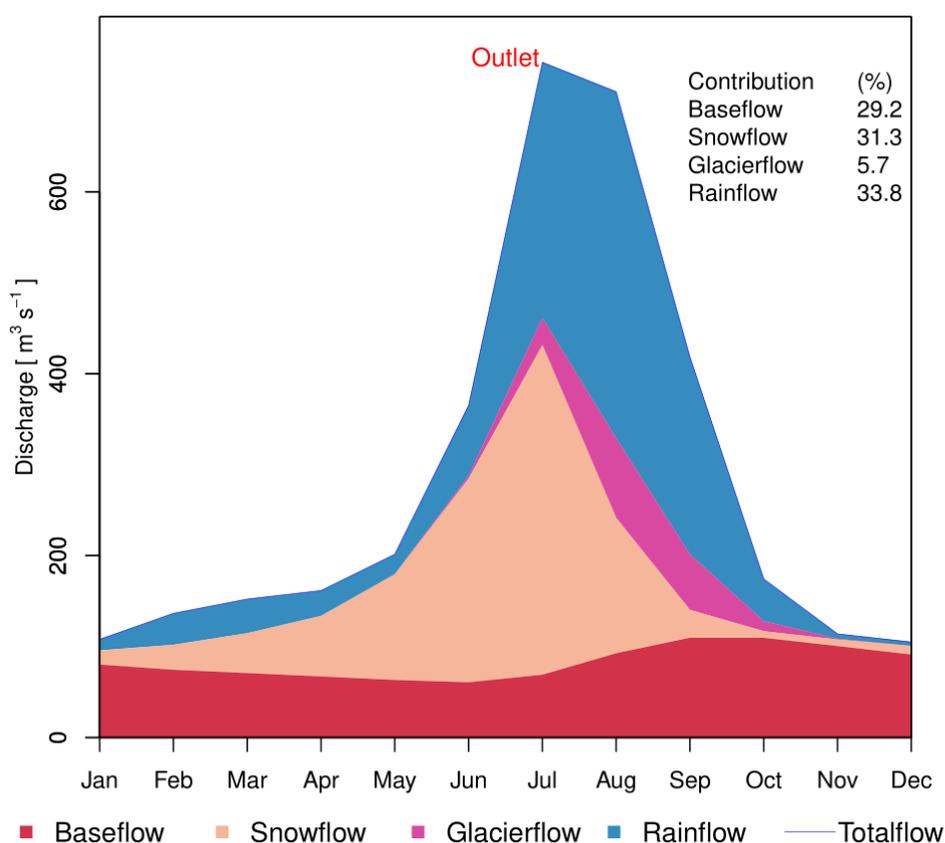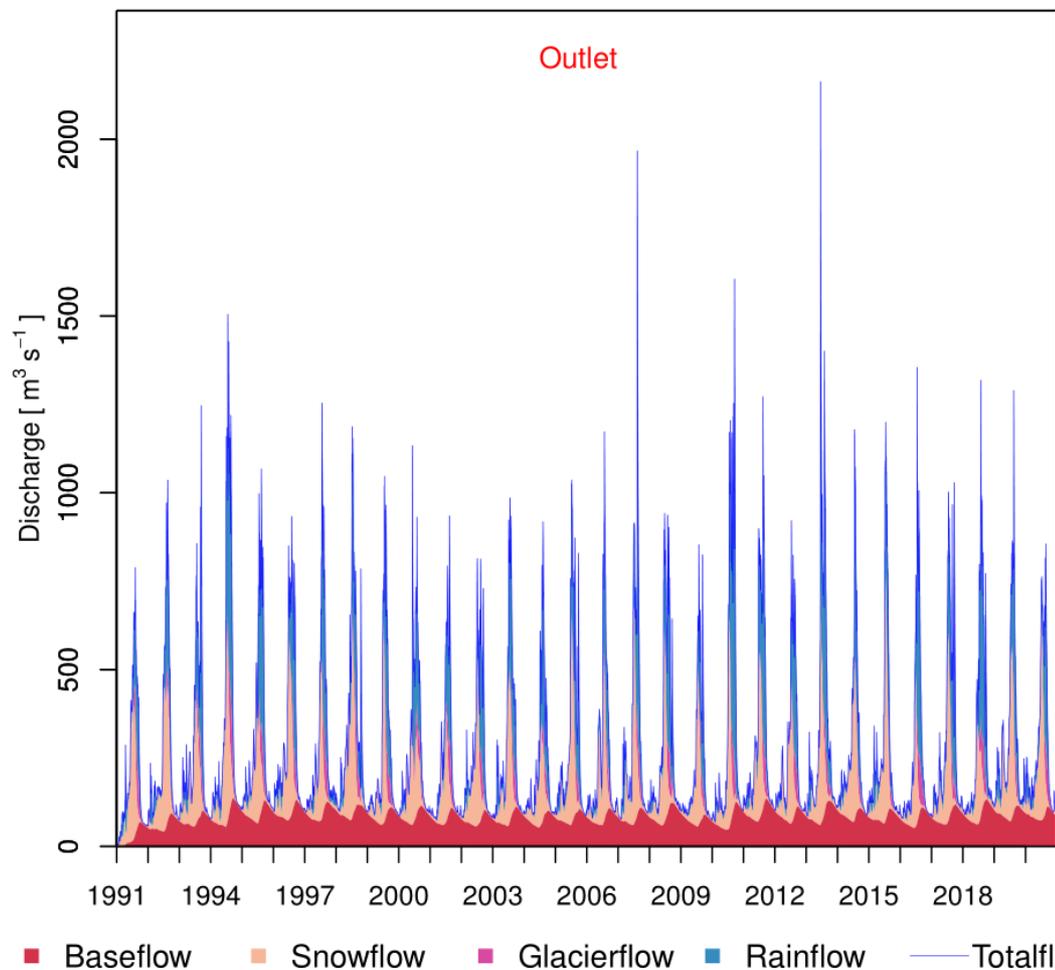
Figure 20. Baseline daily runoff with the distinction of flow components (base, snow, glacier, and rain-runoff) at the outlet of the Bhagirathi river basin (just before the confluence of the Alaknanda River) for 1991–2020.

The linear trends suggest that the total runoff has increased slightly in the past 30 years (Figure 21). This is due to an increase in the rainfall-runoff and baseflow contributions. However, the snow and glacier flow has decreased over the past. This is due to ever increasing temperature in the recent decades. The increase in temperature reduces the solid fraction of the precipitation and thus the snow runoff flow decreases in time. Higher temperature also has been melting away the glacier, and since the glacier area has reduced, the amount of glacier runoff has decreased.
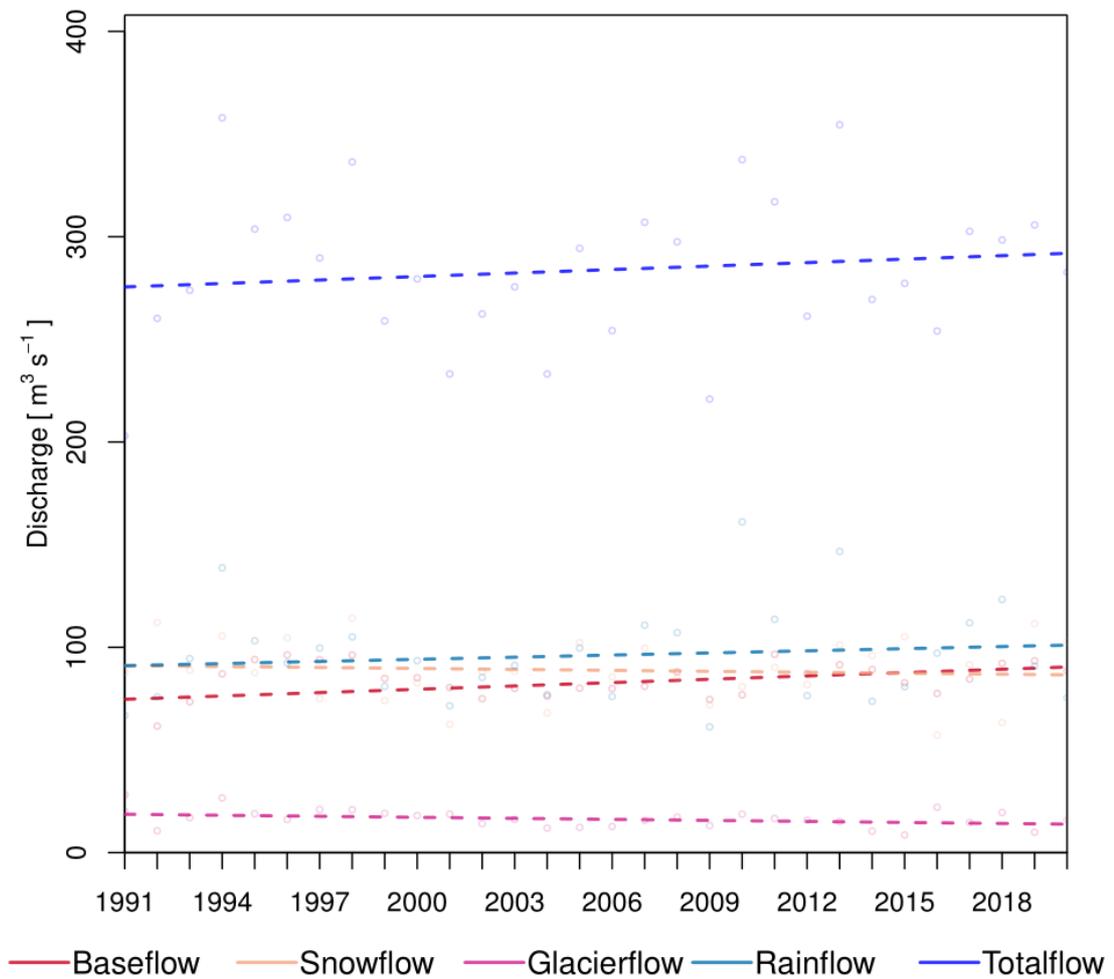
Figure 21. Linear trends of average annual runoff components (base, snow, glacier, and rain-runoff flow) at the outlet of the Bhagirathi river basin (just before the confluence of the Alaknanda river) for 1991–2020.

4.4 Future climate

A subset of the full ensemble of climate change scenarios provided by General Circulation Models (GCMs) in the CMIP6 multi-model ensemble is selected. For a medium and a high temperature increase scenario (i.e., RCP4.5 and RCP7.0), we selected 4 GCM runs each, to represent the full spectrum of projected changes in temperature and precipitation of the full ensemble. For each corner, the three models with the lowest values for D are selected from the ensemble. The initial selection results in three model runs × four corners = 12 model runs for each RCP (Figure 22). Size of dots in Figure 22 reflects the Mean Absolute Error (MAE) for T. Smaller dot means lower MAE and higher skill. The Colour of dots reflects MAE for P. Lighter colour illustrates, lower MAE and higher skill. The skill score was calculated following the below points:

- For mean air temperature and precipitation, the GCM skill is calculated as MAE when comparing monthly climatology of the GCM and baseline forcing dataset. Units are °C for temperature and mm/month for precipitation.
- The period over which the climatology is calculated is 1991-2014. It ends in 2014 because historical runs of the GCMs end after 2014.

FutureWater

- Basin-averaged values are compared and the GCM values are area-weighted for the grid cells in the GCM's native resolution covering the basin.
- For both mean air temperature and monthly precipitation sums the MAE values of the 12 months are averaged.
- MAE values are then scaled between 0 and 1 over the range of MAE values in each ensemble and a combined skill score is calculated by averaging the scaled scores for T and P. Higher values (closer to 1) indicate higher skill.
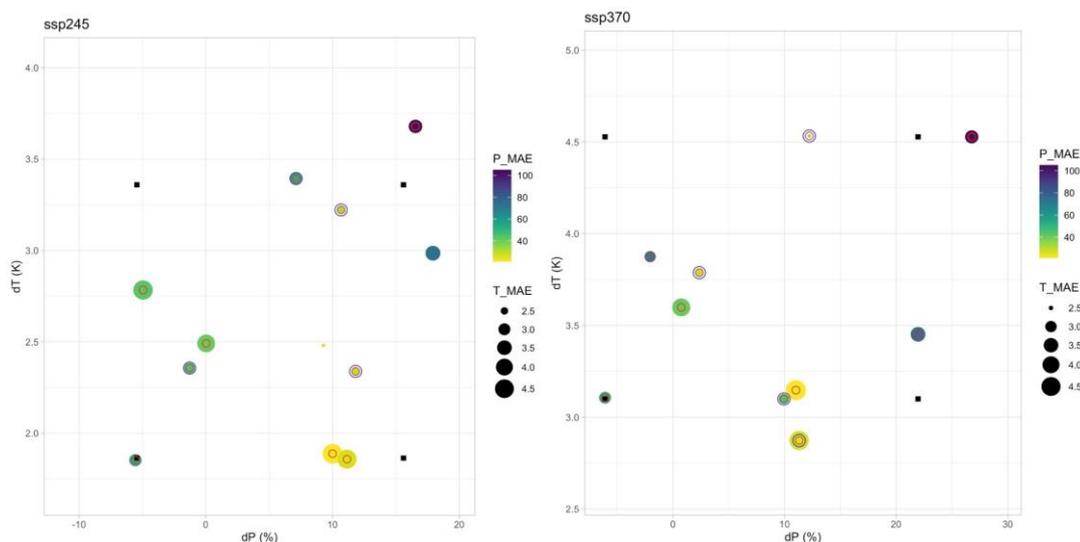
Figure 22. Projected changes in mean air temperature (ΔT) and annual precipitation sum (ΔP) between 2071–2100 and 1985–2014 for all included RCP4.5 (a) and RCP7.0(b) GCM runs. Black squares indicate the 10th and 90th percentile values for ΔT and ΔP. MAE for T (dot size, °C). Smaller dot is lower MAE (higher skill)). MAE for P (colour scale, mm/month). Lower value is higher skill. 3 GCM runs closest to each corner (red circles). Selected GCM runs (blue circles)

For the 3 selected at each corner, we select the GCM run with the highest combined skill score. In addition to representativeness of the projected climate change we make sure to only include GCM runs that have sufficient skill in simulating the historical climate (Table 4).

Table 4. List of selected models. For each model one member is included, 'r1i1p1f1' if available.

Scenario	GCM run	member	ΔT	ΔP	T_MAE (°C)	P_MAE (mm month^{-1})
SSP245	EC-Earth3	r1i1p1f1	3.2	10.7	2.5	32.3
	GFDL-CM4	r1i1p1f1	3.4	7.1	3.0	52.5
	MPI-ESM1-2-HR	r1i1p1f1	2.4	-1.3	2.9	44.8
	AWI-CM-1-1-MR	r1i1p1f1	2.3	11.8	2.6	28.6
SSP370	EC-Earth3	r1i1p1f1	4.5	12.2	2.5	32.3
	AWI-CM-1-1-MR	r1i1p1f1	3.8	2.4	2.6	28.6
	MPI-ESM1-2-HR	r1i1p1f1	3.1	9.9	2.9	44.8
	INM-CM5-0	r1i1p1f1	2.9	11.3	4.6	26.3

To bias correct the future CMIP6 GCM temperature and precipitation forcing and downscale it to the model domain grid, we applied a monthly delta change approach. Downscaling procedure for monthly deltas followed the following procedure:

i. GCM data was resampled to the model grid using bilinear interpolation.
ii. Monthly climatological means (temperature) and sums (precipitation) were calculated for both the GCM data and the baseline series over 1991–2020.
iii. Monthly climatological differences, i.e., deltas, between the GCMs and the baseline data were determined using subtraction (temperature) and division (precipitation).
iv. Future GCM series were downscaled by adding (temperature) or multiplying (precipitation) the resampled daily values with the offsets and scaling factors determined under (3) on a monthly basis. That is, all daily values that correspond to a specific calendar month are multiplied by the same bias correction factor.

Note that the output of the monthly delta change bias correction **includes leap days**. For models that use 365_day calendar type ("GFDL-CM4_ssp245" and "INM-CM5-0_ssp370"), leap days were inserted by copying 28 February to 29 February.

The downscaling and bias correction exercise reveals that the temperature is increasing at a higher rate compared to the precipitation for the Bhagirathi domain (Figure 23 and Figure 24). The temperature has increased at a rate of 0.03 °C yr-1 and 0.044 °C yr-1 for the ssp245 and ssp370 scenario, respectively. This translates to about 2.4 °C and 3.5 °C temperature rise by the end of the century (2100) for ssp245 and ssp370 since 2020. The precipitation increases at a rate of 1.7 and 1.8mm yr-1 for the ssp245 and ssp370 scenarios. The variability in precipitation projection is higher compared to the temperature projection. The differences between the ssp scenarios are smaller for precipitation compared to the temperature. The ssp scenarios deviate notably after 2070.
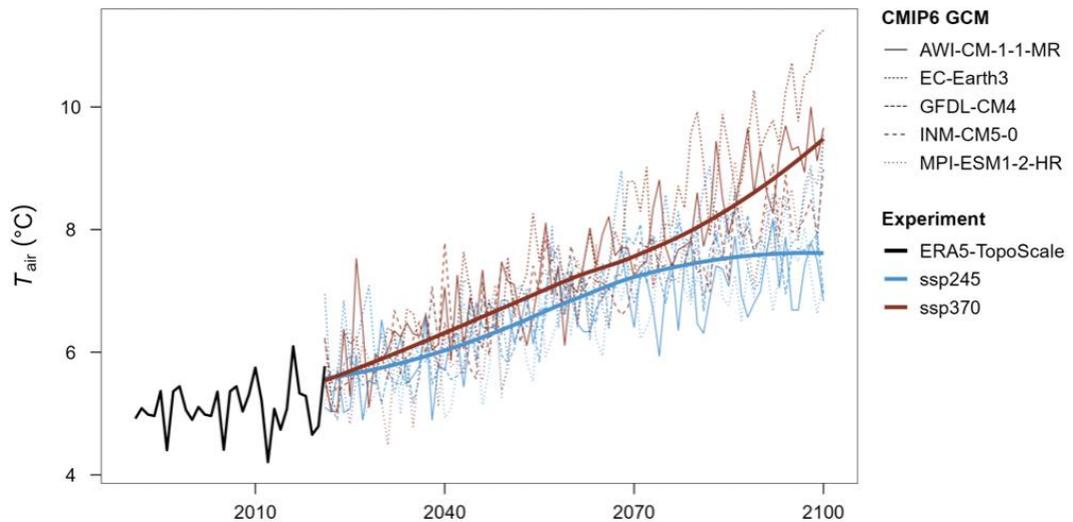
Figure 23. Annual domain-average temperature series of the selected GCMs after bias-correction and downscaling for the Bhagirathi domain. The thick lines show the SSP-RCP ensemble mean signal.
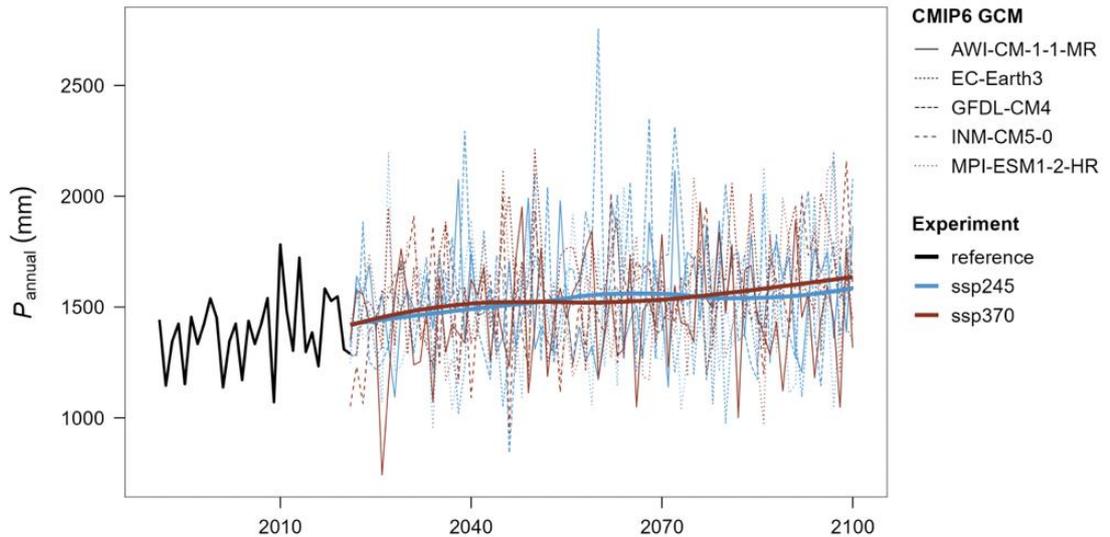
Figure 24. Annual domain-average precipitation series of the selected GCMs after bias-correction and downscaling for the Bhagirathi domain. The thick lines show the SSP-RCP ensemble mean signal.

4.5 Future hydrology

To understand the hydrological changes in the future, different time scales i.e., seasonal and decadal and time slices i.e., mid-century (2036–2065) and end-of-century (2071-2100) are investigated. On a seasonal scale for the mid-century, the total flow increases in both scenarios, i.e., ssp245 and ssp370 (Figure 25). The glacier-melt runoff increases by the mid-century for both ssp scenarios as compared to the baseline. The increase in glacier melt runoff is attributed to the increase in temperature in both ssp scenarios. The rising temperature results in a decreasing fraction of solid precipitation (i.e., snowfall), which consequently results in decreased snowmelt runoff by the mid-century. The rainfall-runoff contribution significantly increases by mid-century for both ssp scenarios. Interestingly, the timing of peak total runoff changes from July to August by the mid-century. The increasing contribution of rainfall-runoff and glacier-melt runoff and decreasing contribution of snow runoff are the prime reasons for the detected shift in peak total runoff from July to August for mid-century.
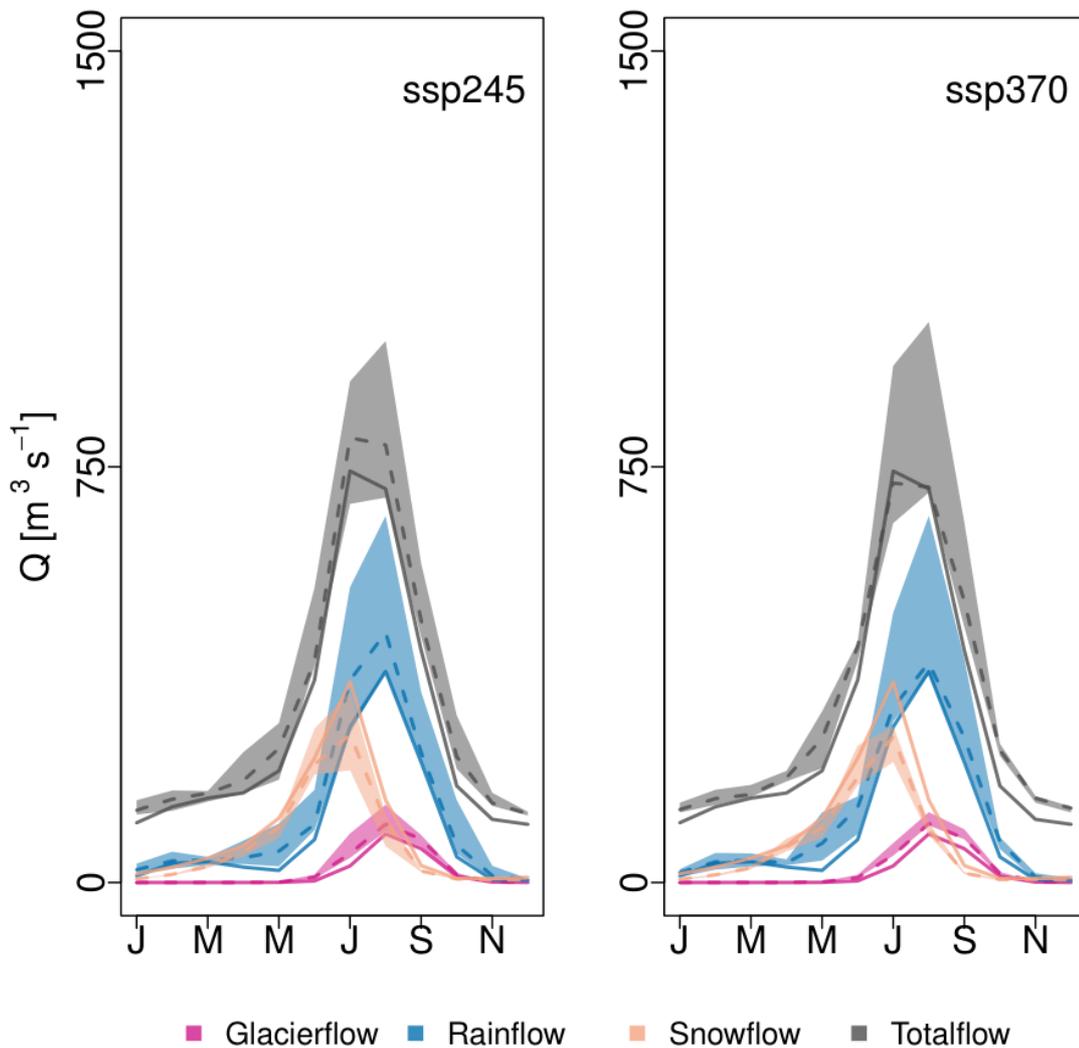
Figure 25. Seasonal changes in the hydrological regime for the mid-century (2036–2065) at the outlet of the Bhagirathi river basin (just before the confluence of the Alaknanda River). The shaded color represents variability (minimum and maximum) of the flow contributors. The dashed and solid colored line represents the median of the four climate models and baseline flow (1991-2020).

For the end-of-century time slice, similar changes are observed (Figure 26). The rainfall-runoff contribution intensifies compared to the mid-century for both ssps. The snow runoff reduces significantly compared to the baseline for the end-of-century. The reduction in snow flow runoff is higher by the end-of-century compared to the mid-century. The increase in glacier melt runoff seen in the mid-century recedes by the end-of-century. This signifies that the peak glacier melt runoff has already been attained by the mid-century and glacier-melt runoff will decline by the end-of-century in the Bhagirathi river basin. The shift in the peak total runoff becomes more evident by the end-of-century for both scenarios.
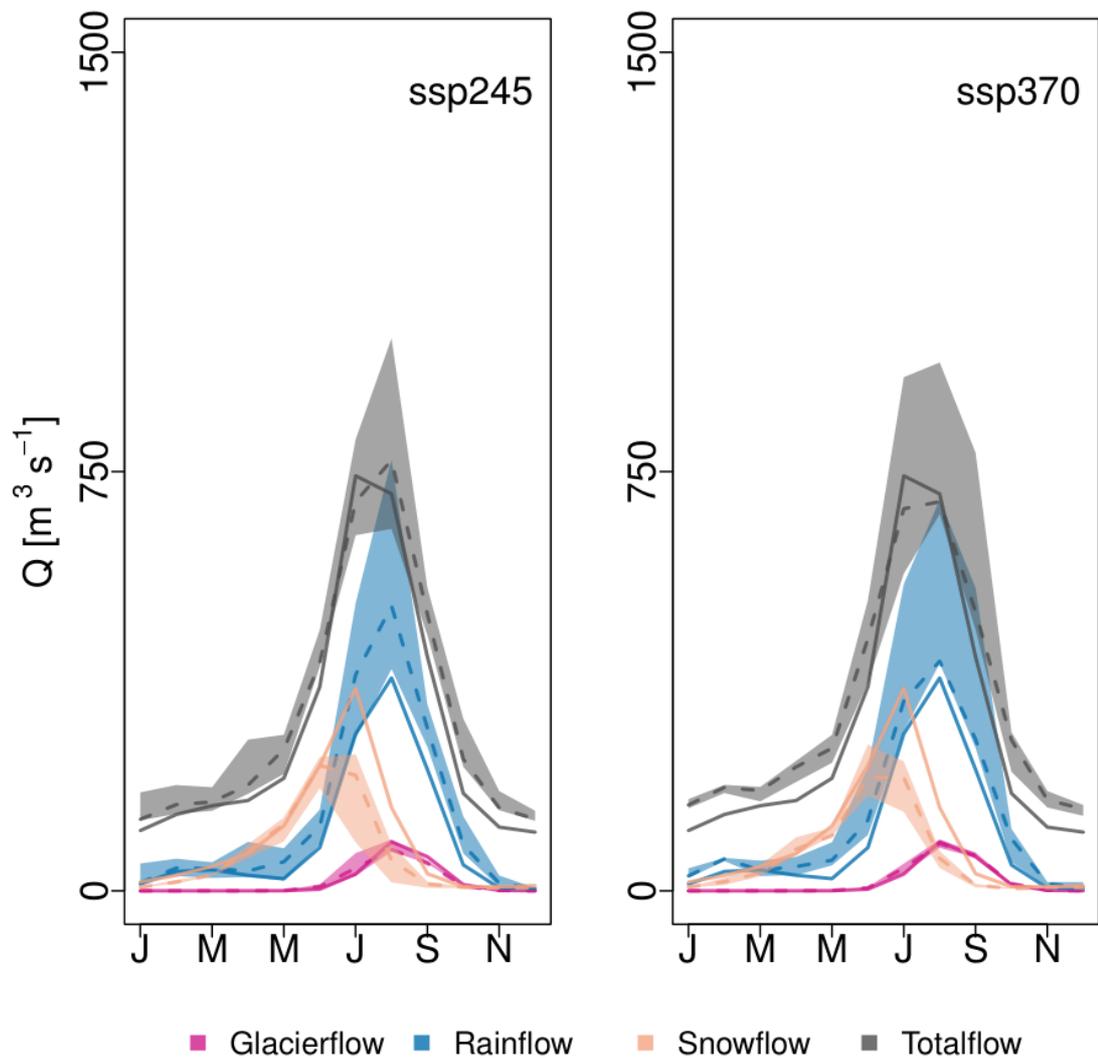
Figure 26. Seasonal changes in the hydrological regime for the end of the century (2071–2100) at the outlet of the Bhagirathi river basin (just before the confluence of the Alaknanda River). The shaded color represents the variability (minimum and maximum) of the flow contributors. The dashed and solid-colored line represents the median of the four climate models and baseline flow (1991-2020).

For the annual scale, snow and glacier melt runoff show a clear declining trend by the end of the century (Figure 27). The rainfall-runoff and baseflow components increase in the future. This increase is attributed to the increased precipitation in the basin. The increase in rainfall-runoff and baseflow components is leveled off by the decline in the snow and glacier melt runoff. So, in the future, the total runoff stays relatively stable for ssp245 and slightly increases for ssp370.

Even though the total flow remains relatively constant for ssp245 and slightly increases for ssp370 by the end of the century, the number of flood waves tends to increase for both ssp245 and ssp370 (Figure 28). The flood wave is defined as the number of days (at least two consecutive days) when the flow is higher than the Q_{85} percentile flow. This increase in flood wave numbers will have severe implications on critical hydraulic (hydropower, irrigation, and water supply) and other infrastructures (road, tunnels, transmission lines, and buildings).
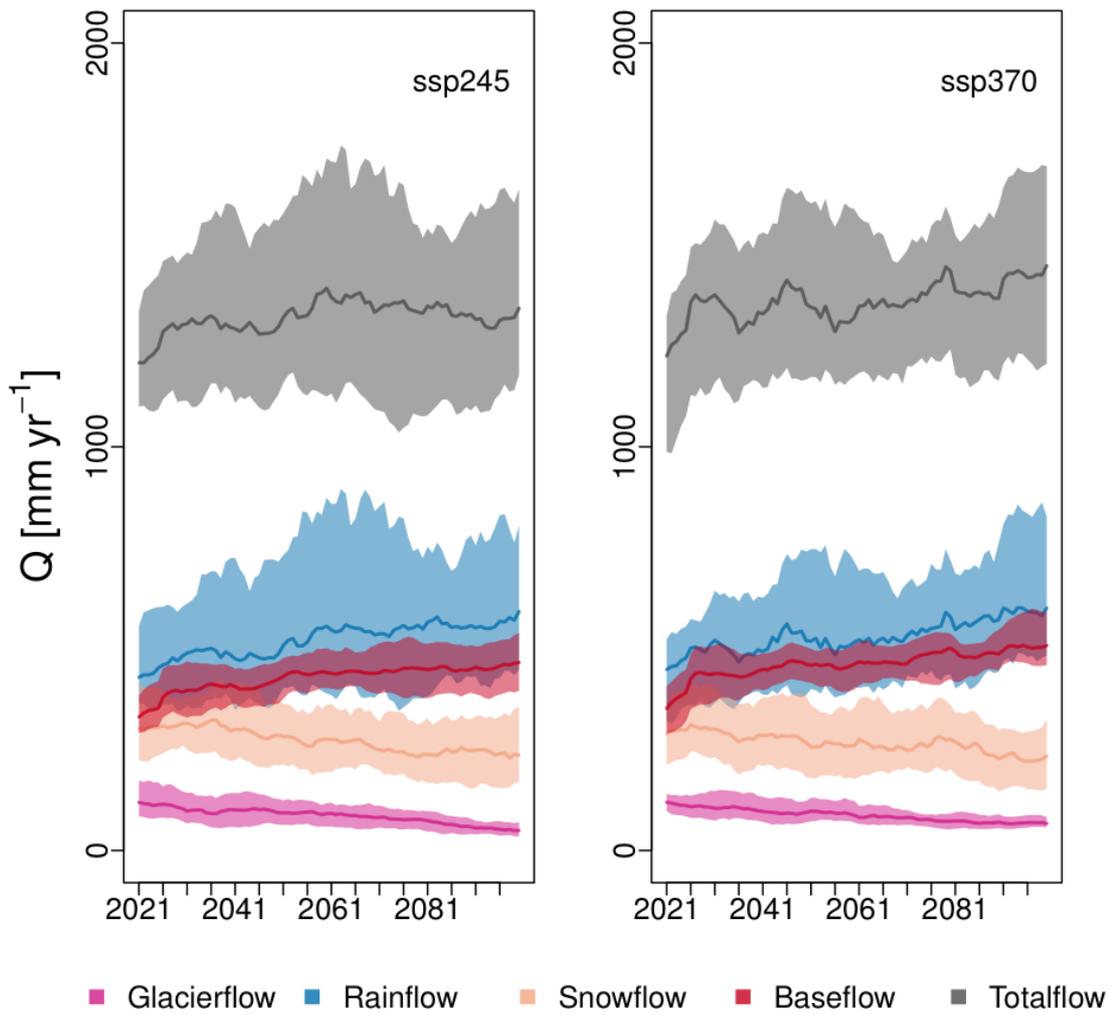
Figure 27. Annual changes in the hydrological fluxes at the outlet of the Bhagirathi river basin (just before the confluence of the Alaknanda River). The shaded color represents the variability (10-year running mean) of the median flow contributors from four climate models. The solid-colored line represents the median of four climate models.
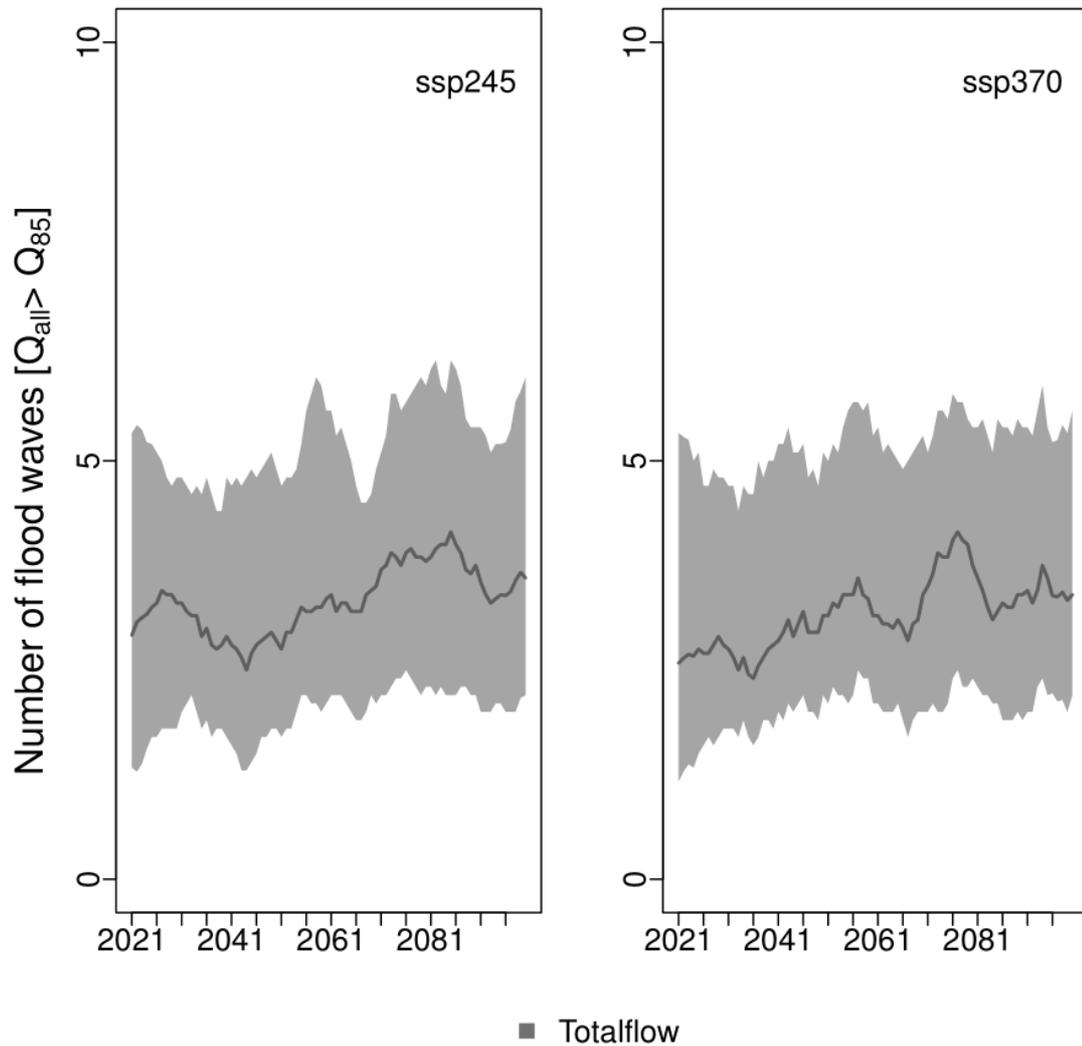
Figure 28. The number of flood waves per year at the outlet of the Bhagirathi river basin (just before the confluence of the Alaknanda river). The shaded color represents the variability (10-year running mean) of the median flow contributors from four climate models. The solid-colored line represents the median of four climate models.

Similar hydrological behavior is observed for the Din Gad catchment (Figure 29). The glacier melt runoff decreases effectively. A smaller decreasing rate is shown for snow runoff, with a visible accelerated decrease after 2070 for ssp370. The rainfall-runoff increases because of higher precipitation and compensates for the reduction in flow due to lower snow and glacier runoff. Going further upstream to higher elevation at Dokriani catchment (Figure 30), since the catchment is more snow and glacier dominated, the modelled decrease in snow and glacier runoff is much larger than the increased rainfall runoff and therefore an apparent decrease of more than 20% in total river flow for the Dokriani catchment is expected.
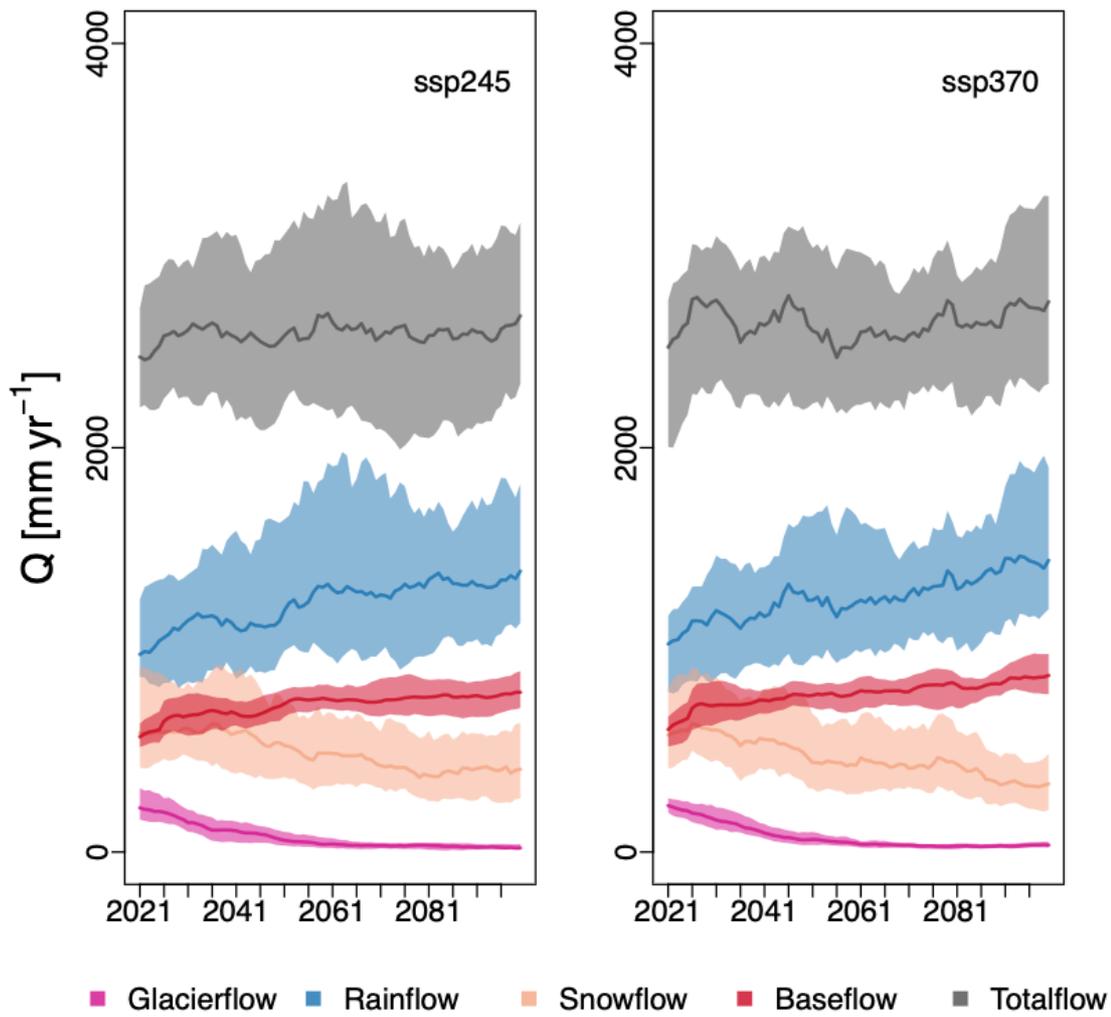
Figure 29. Annual changes in the hydrological fluxes at the outlet of the Din Gad catchment. The shaded color represents the variability (10-year running mean) of the median flow contributors from four climate models. The solid-colored line represents the median of four climate models.
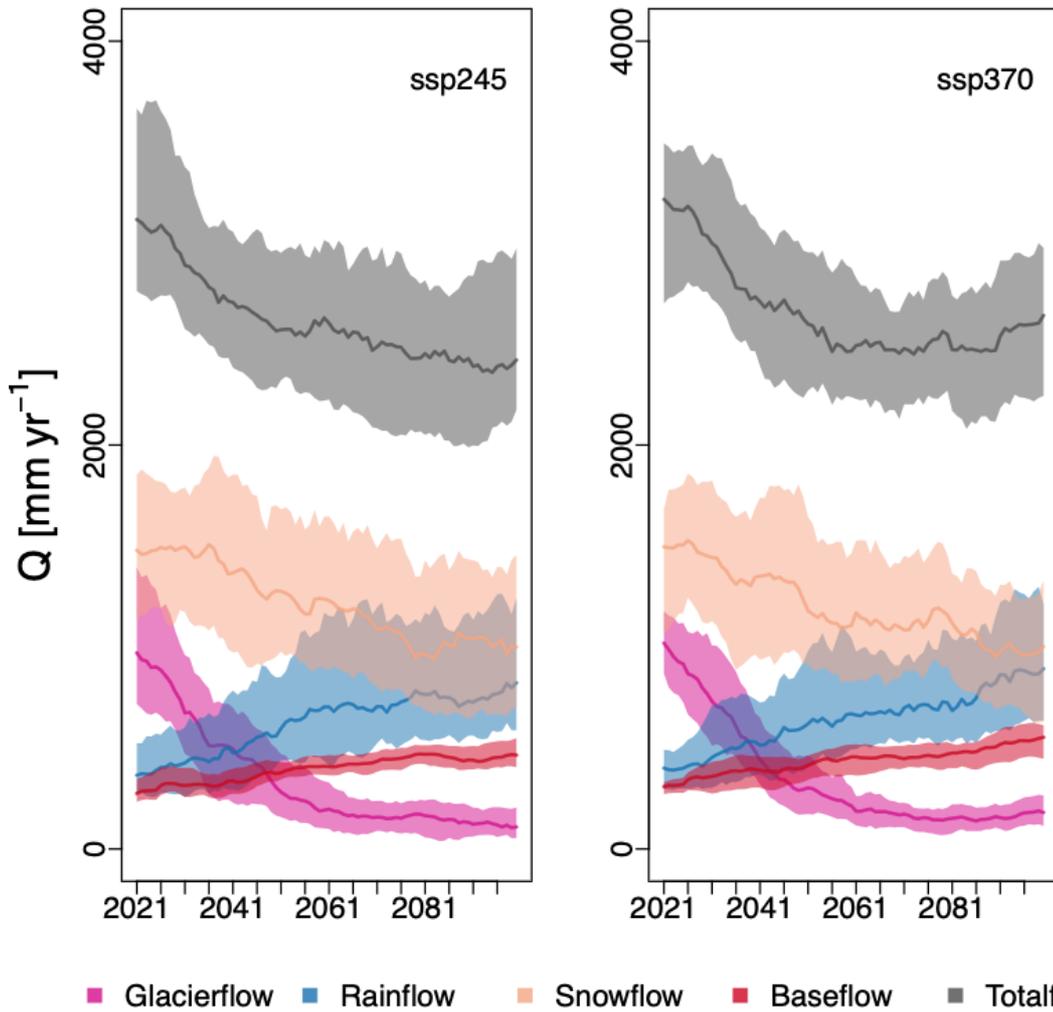
Figure 30. Annual changes in the hydrological fluxes at the outlet of the Dokriani catchment. The shaded color represents the variability (10-year running mean) of the median flow contributors from four climate models. The solid-colored line represents the median of four climate models.

The glacier runoff declines at a faster rate compared to the snow runoff (Figure 30). In the Dokriani catchment, warming results in a higher melt rate per unit glacier area as well as a decline of glacier area. The decline in glacier area is so large (Figure 31) that the higher melt rate does not increase the glacier runoff (Figure 30). Glacier mass balance increases as the warmer climate melts away the ablation area of the Dokriani glacier and higher precipitation adds more snow to its accumulation area. For a warmer scenario as ssp370, after 2070 the temperature is noticeably higher, which decreases the amount of solid precipitation as well as increases the amount of melt, so the glacier accumulation area becomes so small that cannot compensate for the increased melt and therefore the glacier mass balance begins to decrease as the glacier melts away (Figure 31).
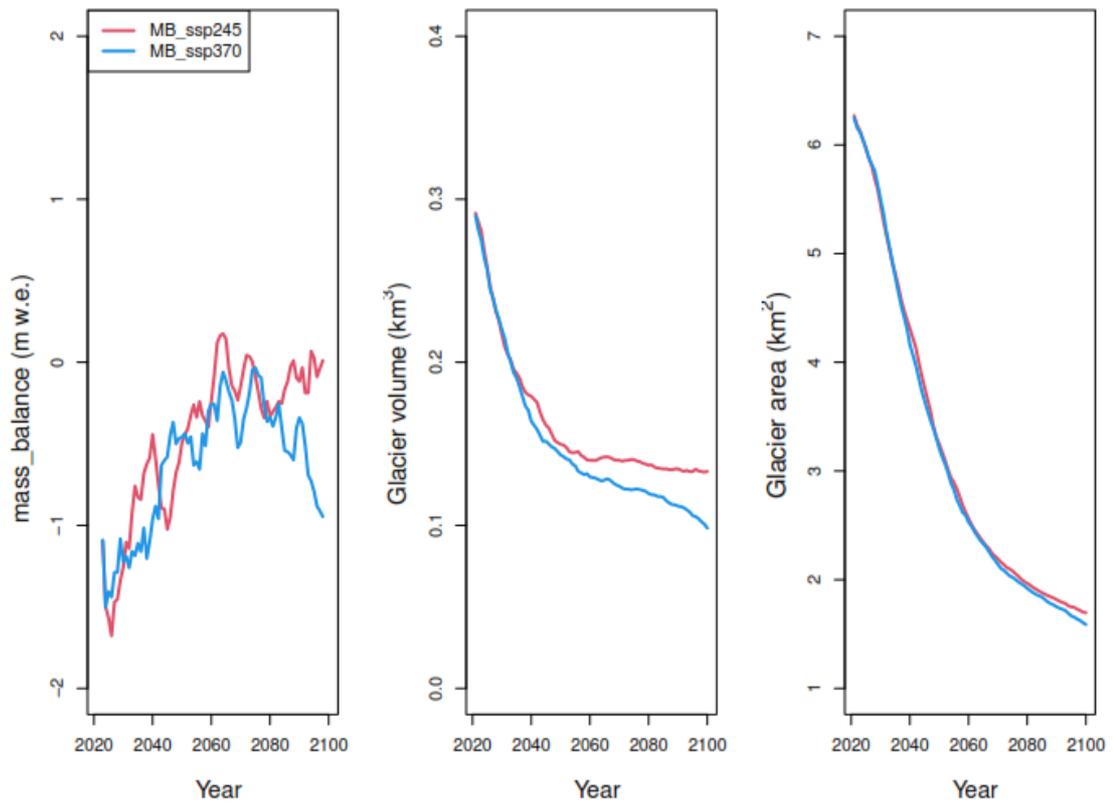
Figure 31. Future Dokriani glacier mass balance and glacier volume. The ssp245 (red) and ssp370 (blue) results are based on the average of the four different downscaled GCM runs.

Looking at the seasonal changes of flow components of the Din Gad and Dokriani catchments at the end of century (Figure 32 and Figure 33, respectively), it reveals that for the Din Gad catchment by the end of century, glacier and snow runoff reduces substantially and the catchment becomes more rainfall dominated. Therefore, the peak in the total flux follows the rainfall runoff pattern and is shifted from July to August.

FutureWater
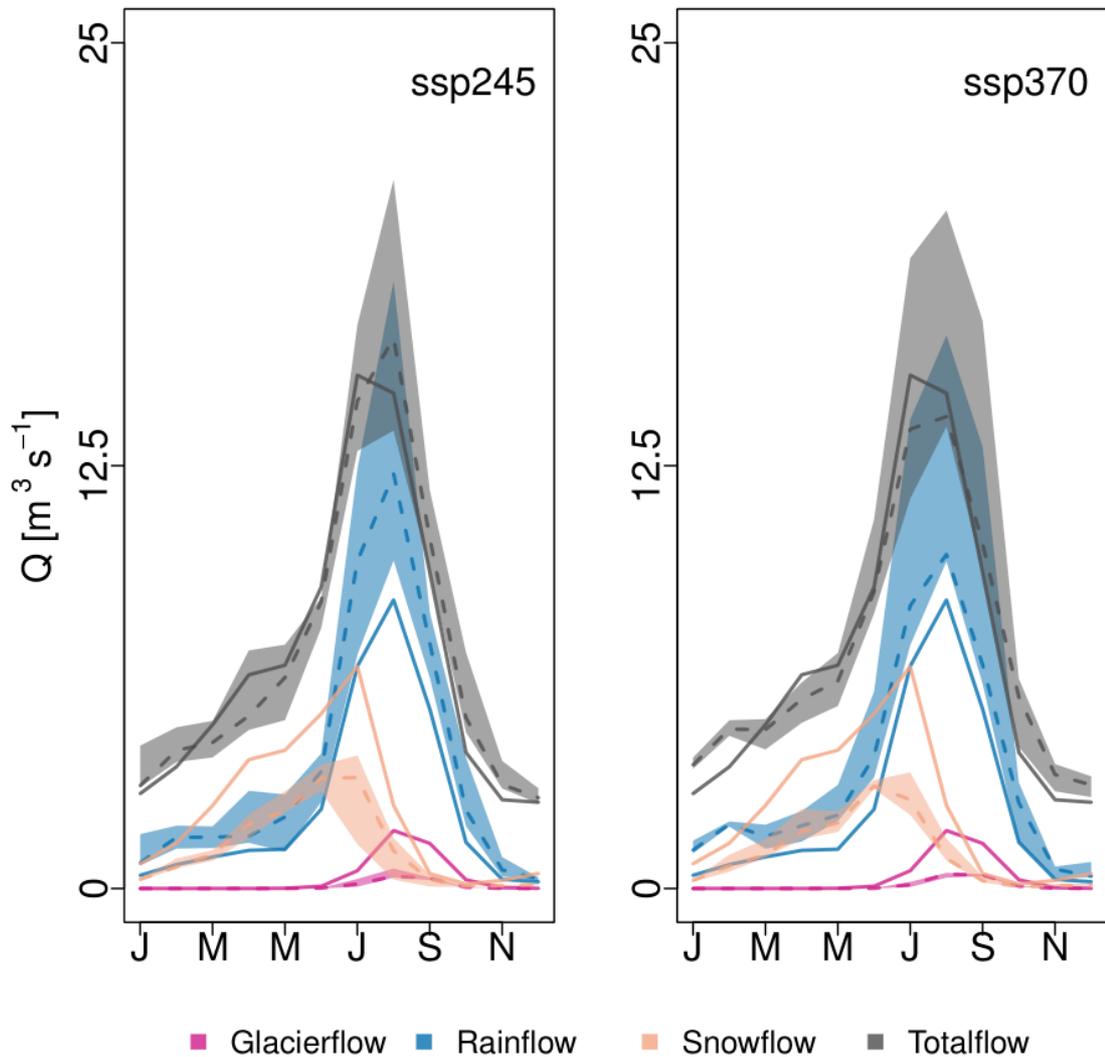
Figure 32. Seasonal changes in the hydrological regime for the end of the century (2071–2100) at the outlet of the Din Gad catchment. The shaded color represents the variability (minimum and maximum) of the flow contributors. The dashed and solid-colored line represent the median of the four climate models and the baseline flow (1991-2020), respectively.

For the Dokriani catchment, which is higher up and half covered by glaciers, even with a substantial decrease in its snow runoff component, the total flow is still dominated by snow runoff. Therefore, the peak flow is not shifted to August but stays high for the whole month of July and August. A decrease in glacier-melt and snow runoff affects the total flux, as the increase in rain is not enough to compensate for the decrease in snow and glacier melt runoff.

Figure 33. Seasonal changes in the hydrological regime for the end of the century (2071–2100) at the outlet of the Dokriani catchment. The shaded color represents the variability (minimum and maximum) of the flow contributors. The dashed and solid-colored line represent the median of the four climate models and the baseline flow (1991-2020), respectively.
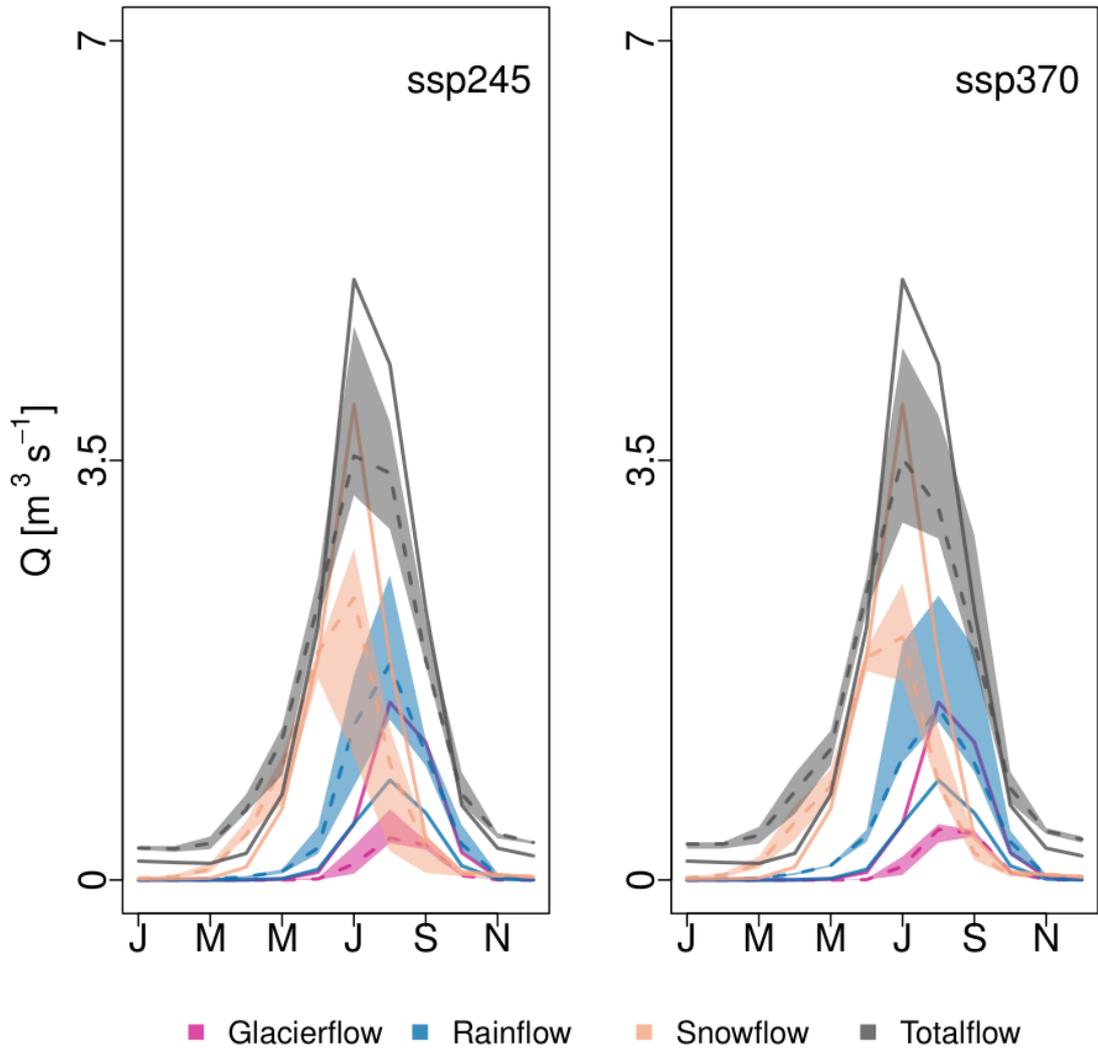
5 Discussion

The results of this study heavily rely on the ERA5 reanalysis data downscaled with TopoSCALE and are therefore subject to limitations in those. The downscaling scheme's main purpose is to correct bias between the large-scale reanalysis and fine-scale model grid, for example, the difference in air temperature due to difference in elevation. However, initial biases in the reanalysis will persist and are related to the density of observations that are assimilated and therefore available to correct the model. Mountains in general, and the Himalayas specifically, tend to be relatively data-poor leading to less well constrained reanalysis data in these regions. A lot of effort has been put into acquiring the local-scale observed data but a major part of those data could not be acquired, specifically for the glacier related data, and therefore, available open source data including satellite data were used for the modelling work, especially for the Din Gad glaciated catchment. Therefore, we used the information from either literature or freely accessible data in the public domain. We combined the data from different open-source platforms to model and validate our results in this project.

It should be noted that the selected future climate models may not cover the full range of uncertainty in future projections of the final CMIP6 ensemble. But the chosen models provide a good indication of the potential range of future changes.

The baseflow runoff depends on the capacity of aquifers, depth of saturated soil column, distribution of permafrost, units of rock, or an unconsolidated soil formation. There is no or little information on aquifers, bedrocks, and other parameters in this region. Thus, the baseflow results of this study may not fully represent the dynamic reality.

5.1 Guidelines

The modeling approach used in this study can be upscaled to the data-scarce regions in the high mountains of Asia. It is a must to have sufficient long-term meteorological (2m air and skin temperature, precipitation, humidity, sub-soil temperature), detailed land use, soil and rock characteristics (both surface and subsurface), and discharge data available for high altitudes regions to perform a proper climate change-impact modeling.

It is important to ensure that the physical processes are well represented in the glacio-hydrological model to be used for the modeling purpose. Thus, we suggest using a 3-step (or multistep) calibration process depending on the availability of the data. In the first step, the glacier mass balance should be parameterized in such a way that it represents the observed mass balance data and glacier dynamics fairly well. In the second step, it should be ensured that the snow processes such as snow depth, snow water equivalent, snow cover area, and snow persistence are fairly represented in the simulation model. Finally, the surface and sub-surface runoff processes should be adjusted in such a way that the simulated discharge is similar to the observed discharge (and other observed variables if available). This modeling approach could be easily adapted to other parts of the Indian Himalayas or elsewhere in the high mountains of Asia. There will be a workshop in November to show in a generic way how the SPHY model can be built and we will also provide online teaching. All the materials and manuals will be made online before the training.

5.2 Recommendations

To lessen the uncertainties and the limitation mentioned above, we recommend to set-up a monitoring project focusing on meteorological observations plus discharge in particular at higher altitudes. This

would help to modify the ERA5 reanalysis data for higher elevation basins and have a more robust calibration of model parameters.

Further improvement in the simulation of physical processes, such as snow avalanching, and snow redistribution is recommended. More research is needed to improve the simulation of the snow module. One of the potential improvements is the assimilation of observed snow information such as snow water equivalent, snow depth, and snow cover area in the modeling exercise for the small-scale Din Gad model.

The glacio-hydrological modeling exercise with SPHY focused mainly on the water availability issues in the region. For the holistic integrated water resources management (IWRM), it is important to address the dynamic demand and supply management scenarios in the future. Allocation of limited water resources in the water-scarce region, issues related to environmental quality, planning under climate variability and uncertainty, and the need to develop and implement sustainable water use strategies are increasingly pressing concerns for water resource planners. Water Evaluation And Planning (WEAP) incorporates these values into a practical tool for water resources planning and policy analysis. The outputs of the detailed SPHY modeling will serve as inputs to the WEAP model to generate different demand-supply scenarios for the future. We recommend to couple outputs of SPHY to WEAP model for a more comprehensive overview of the factors and scenarios that must be considered in managing water resources for present and future use.

5.3 Data availability

The SPHY model codes can be accessed through the GitHub repository (https://github.com/FutureWater/SPHY). All the input files used in the model and results for the baseline period and future runs for both small-scale and large-scale model runs can be found here https://doi.org/10.5281/zenodo.6795100. The ERA5 climate data are acquired from Copernicus Climate Change Service (C3S) Climate Data Store (CDS).

6 Conclusions

Here we use the Spatial Processes in Hydrology (SPHY) model to assess upstream runoff composition in the Bhagirathi river basin and we demonstrate how runoff composition and total runoff volume are expected to change until 2100 by forcing the model with an ensemble of the latest GCM outputs. Results show that for both the Bhagirathi and Din Gad domain the total water availability will be relatively stable for ssp245 and slightly increases for ssp370 by the end of the century.

We show that the climate change response of hydrological processes varies for different catchments (and sub-catchments) in Bhagirathi river basin. For the Dokriani catchment, runoff is generated at a higher altitude and depends mainly on snow and glacier melt runoff, while for the outlet which is at a lower altitude, rainfall-runoff and baseflow processes dominate runoff. For Din Gad which snow and glacier dominated, the decrease in snow and glacier runoff is much larger than the increased rainfall runoff and therefore they show a larger change in total water availability compared to the overall Bhagirathi river basin. This has been suggested for other regions in HMA, the changes in total water availability are larger at higher altitudes than at lower altitudes for the different future scenarios (Khanal et al., 2021).

Even though the total water availability for the whole Bhagirathi river basin slightly increases by the end of the century, the changes in timing and magnitude of peak water availability and seasonality may impose a serious threat on the livelihood of people. It is the change in seasonality and changes in peak melt runoff that will pose the main challenge to be addressed in adapting to future changes in a region where food security, energy security as well as biodiversity, and the livelihoods of many depend on water from the mountains.

7 References

Aalstad, K., Westermann, S., Schuler, T. V., Boike, J. and Bertino, L.: Ensemble-based assimilation of fractional snow-covered area satellite retrievals to estimate the snow distribution at Arctic sites, Cryosphere, 12(1), 247–270, doi:10.5194/TC-12-247-2018, 2018.

Azam, M. F. and Srivastava, S.: Mass balance and runoff modelling of partially debris-covered Dokriani Glacier in monsoon-dominated Himalaya using ERA5 data since 1979, J. Hydrol., 590(October 2019), 125432, doi:10.1016/j.jhydrol.2020.125432, 2020.

Azam, M. F., Kargel, J. S., Shea, J. M., Nepal, S., Haritashya, U. K., Srivastava, S., Maussion, F., Qazi, N., Chevallier, P., Dimri, A. P., Kulkarni, A. V., Cogley, J. G. and Bahuguna, I.: Glaciohydrology of the Himalaya-Karakoram, Science (80-.)., 373(6557), doi:10.1126/SCIENCE.ABF3668/ASSET/7E3B4E6D-4A64-4A36-9CC5-24AF20033A89/ASSETS/IMAGES/LARGE/SCIENCE.ABF3668-FA.JPG, 2021.

Bolch, T., Kulkarni, A., Kääb, A., Huggel, C., Paul, F., Cogley, J. G., Frey, H., Kargel, J. S., Fujita, K., Scheel, M., Bajracharya, S. and Stoffel, M.: The state and fate of himalayan glaciers, Science (80-.)., 336(6079), 310–314, doi:10.1126/science.1215828, 2012.

Cao, B., Gruber, S., Zheng, D. and Li, X.: The ERA5-Land Soil-Temperature Bias in Permafrost Regions, , (April), 1–22, 2020.

Dobhal, D. P., Pratap, B., Bhambri, R. and Mehta, M.: Mass balance and morphological changes of Dokriani Glacier (1992–2013), Garhwal Himalaya, India, Quat. Sci. Adv., 4, 100033, doi:10.1016/J.QSA.2021.100033, 2021.

Eekhout, J. P. C., Terink, W. and De Vente, J.: Assessing the large-scale impacts of environmental change using a coupled hydrology and soil erosion model, Earth Surf. Dyn., 6(3), 687–703, doi:10.5194/esurf-6-687-2018, 2018.

Farinotti, D., Huss, M., Fürst, J. J., Landmann, J., Machguth, H., Maussion, F. and Pandit, A.: A consensus estimate for the ice thickness distribution of all glaciers on Earth, Nat. Geosci., 12(3), 168–173, doi:10.1038/s41561-019-0300-3, 2019.

Farr, T. G., Rosen, P. A., Caro, E., Crippen, R., Duren, R., Hensley, S., Kobrick, M., Paller, M., Rodriguez, E., Roth, L., Seal, D., Shaffer, S., Shimada, J., Umland, J., Werner, M., Oskin, M., Burbank, D. and Alsdorf, D.: The Shuttle Radar Topography Mission, Rev. Geophys., 45(2), doi:10.1029/2005RG000183, 2007.

Fiddes, J. and Gruber, S.: TopoSCALE v.1.0: Downscaling gridded climate data in complex terrain, Geosci. Model Dev., 7(1), 387–405, doi:10.5194/gmd-7-387-2014, 2014.

Fiddes, J., Endrizzi, S. and Gruber, S.: Large-area land surface simulations in heterogeneous terrain driven by global data sets: Application to mountain permafrost, Cryosphere, 9(1), 411–426, doi:10.5194/TC-9-411-2015, 2015.

Fiddes, J., Aalstad, K. and Westermann, S.: Hyper-resolution ensemble-based snow reanalysis in mountain regions using clustering, Hydrol. Earth Syst. Sci., 23(11), 4717–4736, doi:10.5194/HESS-23-4717-2019, 2019.

Gardelle, J., Berthier, E., Arnaud, Y. and Kääb, A.: Region-wide glacier mass balances over the Pamir-Karakoram-Himalaya during 1999–2011, Cryosphere, 7(4), 1263–1286, doi:10.5194/tc-7-1263-2013, 2013.

Garg, P. K., Yadav, J. S., Rai, S. K. and Shukla, A.: Mass balance and morphological evolution of the Dokriani Glacier, central Himalaya, India during 1999–2014, Geosci. Front., 13(1), 101290, doi:10.1016/J.GSF.2021.101290, 2022.

Hall, D. K. and Riggs, G. A.: MODIS/Terra Snow Cover Monthly L3 Global 0.05Deg CMG Dataset Version 6, https://nsidc.org/data/MOD10CM, 2015.

Hall, D. K., Riggs, G. A., Digirolamo, N. E. and Bayr, K. J.: MODIS Snow-Cover Products, Remote Sens. Environ., 83, 88–89, 2002.

Hargreaves, G. and Samani, Z.: Reference Crop Evapotranspiration from Temperature, Appl. Eng. Agric., 1(2), 96–99, doi:10.13031/2013.26773, 1985.

Hersbach, H., Bell, B., Berrisford, P., Hirahara, S., Horányi, A., Muñoz-Sabater, J., Nicolas, J., Peubey, C., Radu, R., Schepers, D., Simmons, A., Soci, C., Abdalla, S., Abellan, X., Balsamo, G., Bechtold, P., Biavati, G., Bidlot, J., Bonavita, M., De Chiara, G., Dahlgren, P., Dee, D., Diamantakis, M., Dragani, R., Flemming, J., Forbes, R., Fuentes, M., Geer, A., Haimberger, L., Healy, S., Hogan, R. J., Hólm, E., Janisková, M., Keeley, S., Laloyaux, P., Lopez, P., Lupu, C., Radnoti, G., de Rosnay, P., Rozum, I., Vamborg, F., Villaume, S. and Thépaut, J. N.: The ERA5 global reanalysis, Q. J. R. Meteorol. Soc., 146(730), 1999–2049, doi:10.1002/qj.3803, 2020.

Hock, R.: Temperature index melt modelling in mountain areas, J. Hydrol., 282(1–4), 104–115, doi:10.1016/S0022-1694(03)00257-9, 2003.

Houze, R. A., McMurdie, L. A., Rasmussen, K. L., Kumar, A. and Chaplin, M. M.: Multiscale aspects of the storm producing the June 2013 flooding in Uttarakhand, India, Mon. Weather Rev., 145(11), 4447–4466, doi:10.1175/MWR-D-17-0004.1, 2017.

Ji, P. and Yuan, X.: Underestimation of the Warming Trend over the Tibetan Plateau during 1998–2013 by Global Land Data Assimilation Systems and Atmospheric Reanalyses, J. Meteorol. Res., 34(1), 88–100, doi:10.1007/s13351-020-9100-3, 2020.

Kargel, J. S., Leonard, G. J., Bishop, M. P., Kääb, A. and Raup, B. H.: Global land ice measurements from space, Springer., 2014.

Karssenberg, D., Schmitz, O., Salamon, P., Jong], K. [de and Bierkens, M. F. P.: A software framework for construction of process-based stochastic spatio-temporal models and data assimilation, Environ. Model. Softw., 25(4), 489–502, doi:https://doi.org/10.1016/j.envsoft.2009.10.004, 2010.

Khanal, S., Lutz, A. F., Kraaijenbrink, P. D. A., van den Hurk, B., Yao, T. and Immerzeel, W. W.: Variable 21st Century Climate Change Response for Rivers in High Mountain Asia at Seasonal to Decadal Time Scales, Water Resour. Res., 57(5), e2020WR029266, doi:10.1029/2020wr029266, 2021.

Kirches, G., Brockmann, C., Boettcher, M., Peters, M., Bontemps, S., Lamarche, C., Schlerf, M., Santoro, M. and Defourny, P.: Land cover cci-product user guide-version 2, ESA Public Doc. CCI-LC-PUG, (2.4), 2014.

Kraaijenbrink, P. D. A., Bierkens, M. F. P., Lutz, A. F. and Immerzeel, W. W.: Impact of a global temperature rise of 1.5 degrees Celsius on Asia's glaciers, Nature, 549, 257 [online] Available from: https://doi.org/10.1038/nature23878, 2017.

Kumar, A., Verma, A., Dobhal, D. P., Mehta, M. and Kesarwani, K.: Climatic control on extreme sediment transfer from Dokriani Glacier during monsoon, Garhwal Himalaya (India), J. Earth Syst. Sci. 2014 1231, 123(1), 109–120, doi:10.1007/S12040-013-0375-Y, 2014.

Kumar, S.: Stories of Impact Flood Damage in Uttarakhand, Glob. Facil. Disaster Reduct. Recover., 2 pp----2 pp [online] Available from: http://documents.worldbank.org/curated/en/724891468188654600/pdf/97332-BRI-STORIES-OF-IMPACT-Box391466B-PUBLIC-gfdrr-stories-of-impact-uttarakhand.pdf, 2013.

Liang, X., Lettenmaier, D. P., Wood, E. F. and Burges, S. J.: A simple hydrologically based model of land surface water and energy fluxes for general circulation models, J. Geophys. Res., 99(D7), 14415–14428, doi:10.1029/94jd00483, 1994.

Lutz, A. F., Immerzeel, W. W., Shrestha, A. B. and Bierkens, M. F. P.: Consistent increase in High Asia ' s runo due to increasing glacier melt and precipitation, Nat. Clim. Chang., (June), 1–6, doi:10.1038/NCLIMATE2237, 2014.

Lutz, A. F., ter Maat, H. W., Biemans, H., Shrestha, A. B., Wester, P. and Immerzeel, W. W.: Selecting representative climate models for climate change impact studies: an advanced envelope-based selection approach, Int. J. Climatol., 36, 3988–4005, 2016.

Obu, J., Westermann, S., Bartsch, A., Berdnikov, N., Christiansen, H. H., Dashtseren, A., Delaloye, R., Elberling, B., Etzelmüller, B., Kholodov, A., Khomutov, A., Kääb, A., Leibman, M. O., Lewkowicz, A. G., Panda, S. K., Romanovsky, V., Way, R. G., Westergaard-Nielsen, A., Wu, T., Yamkhin, J. and Zou, D.: Northern Hemisphere permafrost map based on TTOP modelling for 2000–2016 at 1 km2 scale, Earth-Science Rev., 193, 299–316, doi:10.1016/J.EARSCIREV.2019.04.023, 2019.

Obu, J., Westermann, S., Vieira, G., Abramov, A., Ruby Balks, M., Bartsch, A., Hrbáček, F., Kääb, A. and Ramos, M.: Pan-Antarctic map of near-surface permafrost temperatures at 1 km2 scale, Cryosphere, 14(2), 497–519, doi:10.5194/tc-14-497-2020, 2020.

Orr, E. N., Owen, L. A., Saha, S. and Caffee, M. W.: Rates of rockwall slope erosion in the upper Bhagirathi catchment, Garhwal Himalaya, Earth Surf. Process. Landforms, 44(15), 3108–3127, doi:10.1002/esp.4720, 2019.

Orsolini, Y., Wegmann, M., Dutra, E., Liu, B., Balsamo, G., Yang, K., Rosnay, P. De, Zhu, C., Wang, W., Senan, R. and Arduini, G.: Evaluation of snow depth and snow cover over the Tibetan Plateau in global reanalyses using in situ and satellite remote sensing observations, , 2221–2239, 2019.

Pellicciotti, F., Buergi, C., Immerzeel, W. W., Konz, M. and Shrestha, A. B.: Challenges and uncertainties in hydrological modeling of remote hindu KushKarakoramHimalayan (HKH) Basins: Suggestions for calibration strategies, Mt. Res. Dev., 32(1), 39–50, doi:10.1659/MRD-JOURNAL-D-11-00092.1, 2012.

Rai, S. P., Purushothaman, P., Kumar, B., Jacob, N. and Rawat, Y. S.: Stable isotopic composition of precipitation in the River Bhagirathi Basin and identification of source vapour, Environ. Earth Sci., 71(11), 4835–4847, doi:10.1007/s12665-013-2875-0, 2014.

Raina, V. K., Srivastava, D. and of India, G. S.: Glacier Atlas of India, Geological Society of India. [online] Available from: https://books.google.nl/books?id=5Q6ObwAACAAJ, 2008.

Rehman, S., Sajjad, H., Masroor, M., Rahaman, M. H., Roshani, Ahmed, R. and Sahana, M.: Assessment of evidence-based climate variability in Bhagirathi sub-basin of India: a geostatistical analysis, Acta Geophys., 70(1), 445–463, doi:10.1007/s11600-022-00726-6, 2022.

Scherler, D., Bookhagen, B. and Strecker, M. R.: Spatially variable response of Himalayan glaciers to climate change affected by debris cover, Nat. Geosci., 4(3), 156–159, doi:10.1038/ngeo1068, 2011.

Shean, D. E., Bhushan, S., Montesano, P. M., Rounce, D., Arendt, A. and Osmanoglu, B.: A systematic, regional assessment of High-Mountain Asia glacier mass balance, Front. Earth Sci., 7, 363: 1–19, 2020.

Simons, G., Koster, R. and Droogers, P.: HiHydroSoil v2 . 0 - High Resolution Soil Maps of Global Hydraulic Properties, , (October), 1–18, 2020.

Srivastava, S., Garg, P. K. and Azam, M. F.: Seven Decades of Dimensional and Mass Balance Changes on Dokriani Bamak and Chhota Shigri Glaciers, Indian Himalaya, Using Satellite Data and Modelling, J. Indian Soc. Remote Sens. 2021 501, 50(1), 37–54, doi:10.1007/S12524-021-01455-X, 2021.

Terink, W., Lutz, A. F., Simons, G. W. H., Immerzeel, W. W. and Droogers, P.: SPHY v2 . 0 : Spatial Processes in HYdrology, , 2009–2034, doi:10.5194/gmd-8-2009-2015, 2015.

Thayyen, R. J., Gergan, J. T. and Dobhal, D. P.: Monsoonal control on glacier discharge and hydrograph characteristics, a case study of Dokriani Glacier, Garhwal Himalaya, India, J. Hydrol., 306(1–4), 37–49, doi:10.1016/J.JHYDROL.2004.08.034, 2005.

Thayyen, R. J., Gergan, J. T. and Dobhal, D. P.: Role of glaciers and snow cover on headwater river hydrology in monsoon regime — Micro-scale study of Din Gad catchment, Garhwal Himalaya, India, Curr. Sci., 92(3), 376–382 [online] Available from: http://www.jstor.org/stable/24096736 (Accessed 27 June 2022), 2007.

Vikhamar Schuler, T. and Østby, T. rn I.: Sval-Imp: A gridded forcing dataset for climate change impact research on Svalbard, Earth Syst. Sci. Data, 12(2), 875–885, doi:10.5194/ESSD-12-875-2020, 2020.

Westermann, S., Ostby, T. I., Gisnäs, K., Schuler, T. V. and Etzelmüller, B.: A ground temperature map of the North Atlantic permafrost region based on remote sensing and reanalysis data, Cryosphere, 9(3), 1303–1319, doi:10.5194/TC-9-1303-2015, 2015.

Wijngaard, R. R., Lutz, A. F., Nepal, S., Khanal, S., Pradhananga, S., Shrestha, A. B. and Immerzeel, W. W.: Future changes in hydro-climatic extremes in the Upper Indus, Ganges, and Brahmaputra River basins, PLoS One, 12(12), e0190224, 2017.

Yadav, J. S., Pratap, B., Gupta, A. K., Dobhal, D. P., Yadav, R. B. S. and Tiwari, S. K.: Spatio-temporal variability of near-surface air temperature in the Dokriani glacier catchment (DGC), central Himalaya, Theor. Appl. Climatol. 2018 1363, 136(3), 1513–1532, doi:10.1007/S00704-018-2544-Z, 2018.

Yan, Z. L., Bian, Q., Xu, Z., Zhao, L., Zhang, Y. F., Zheng, H., Shi, C., Zhang, S. and Xie, C.: Evaluation and intercomparison of multiple snow water equivalent products over the tibetan plateau, J. Hydrometeorol., 20(10), 2043–2055, doi:10.1175/JHM-D-19-0011.1, 2019.
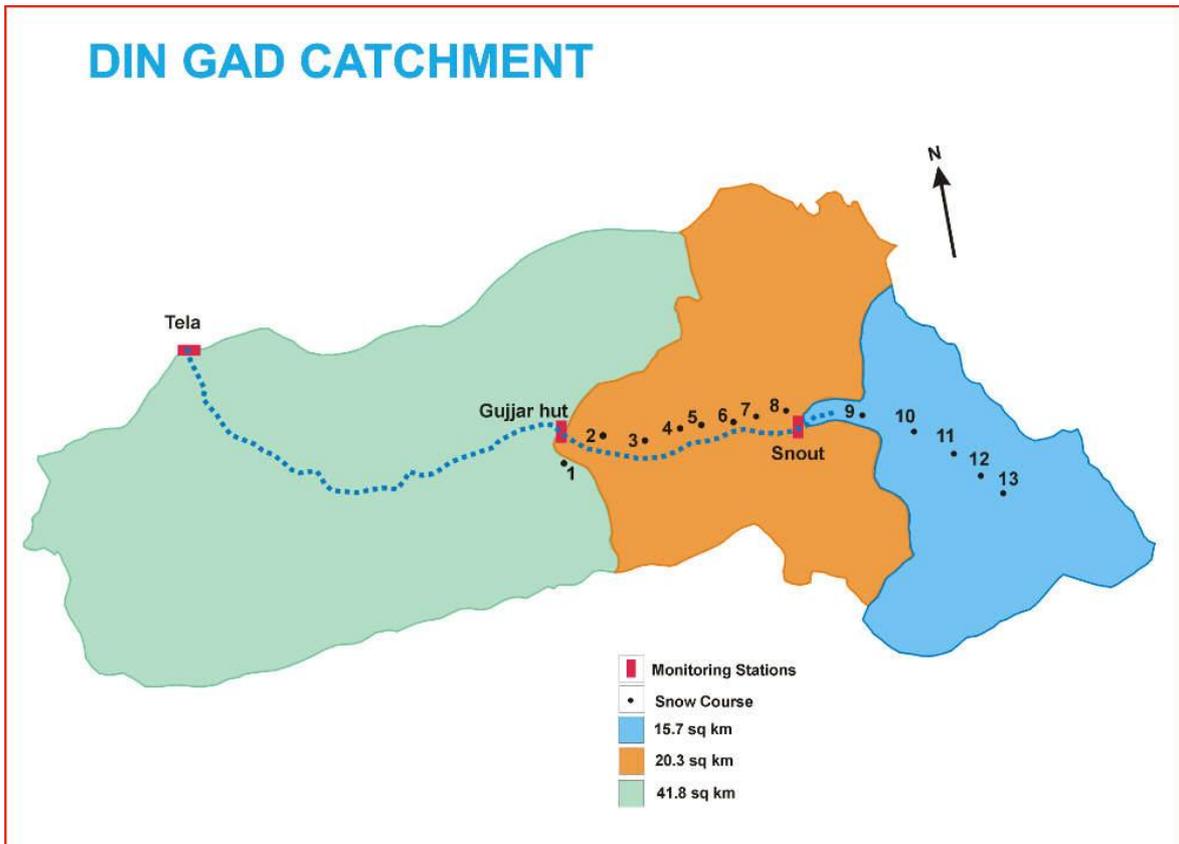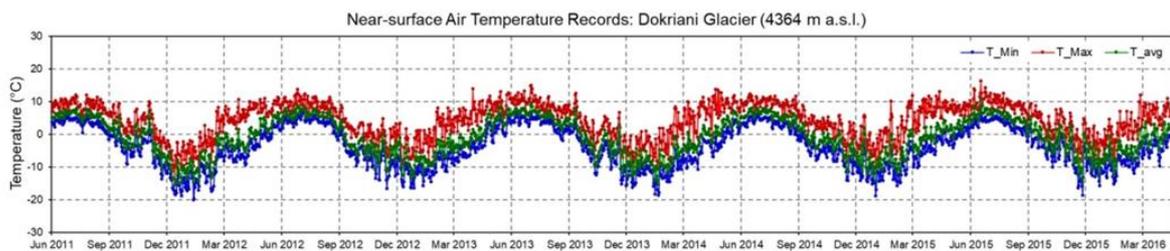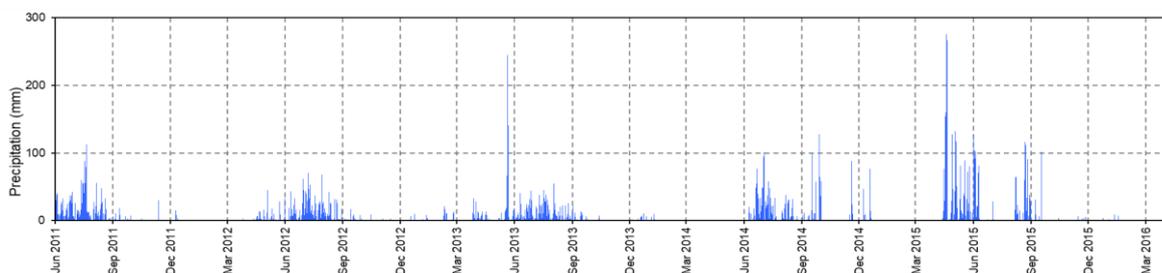
8 Annex

Figure A1. Dokriani glacier and Din Gad catchment and key locations within the basin.

Figure A2. Monthly Average Air Temperature (a) and rainfall (b) records – Dokriani Glacier (4364 m a.s.l. Advance base Camp) 01 July 2011 – 30 April 2016.

Table A1. Snow and glacier melt contribution of various rivers in the IHR.

Rivers	Location	Average snow and glacier melt contribution	References
Chenab	Akhnoor	49%	Singh et al., 1997
Ganga	Devprayag	28%	Singh et al., 1994
Ganga	Rishikesh	40%	Mauraya et al., 2010
Satluj (Indian Part)	Bhakra Dam	68%	Singh and Jain, 2002
Beas	Pandoh Dam	35%	Kumar et al., 2007
Dhauliganga	Tapovan	77%	Arora et al., 2010
Din gad river (Dokriani) Glacier)	Snout	57-86%	Thayyen et al., 2007
Bhagirathi	Bhojwasa	~97%	Singh et al., 2008

Kumar, V. Singh, P., and Singh, V. (2007). Snow and glacier melt contribution in the Beas River at Pandoh Dam, Himachal Pradesh, India, Hydrological Sciences Journal, 52, 376-388.

Singh, P., Haritashya, U. K., and Kumar, N. (2008). Modelling and estimation of different components of streamflow for Gangotri Glacier basin, Himalayas". Hydrological Sciences Journal, 53, 309-322.

Singh, P., and Jain, S. K. (2002). "Snow and glacier melt in the Satluj river at Bhakra Dam in the Western Himalayan region". Hydrological Sciences Journal, 47, 93-106.

Singh, P., Jain, S. K., Kumar, N., and Singh, U. K. (1994). "Snow and glacier contribution in the Ganga river at Devprayag". CS(AR) 132, NIH, Roorkee, 1993-94.

Singh, P., Jain, S. K., and Kumar, N. (1997). "Estimation of snow and glacier melt runoff contribution in the Chenab River at Akhnoor". Mountain Research Development, 17, 49-56.